Dear editor and reviewer,

Thank you for your positive comments and very important recommendations to improve our manuscript. We have carefully modified the manuscript based on your suggestions and provide a response to each comment. Reviewer comments are given in black, and responses are given in blue. Below we provide a marked-up manuscript version showing the changes based on your comments. The main modifications to the manuscript are as follows:

1. Fig. 10 and Table 7 were revised according to your suggestions.
2. We revised the description in Abstract, Section 4.2 and, Section 5 accordingly.
3. We change the term of "Total SWE" to "snow mass" in whole manuscript

Please see below the detailed responses (in blue color).

REVIEWER 1#

In this manuscript, the authors use a support vector regression (SVR) algorithm that they developed in a previous paper to estimate snow depth from passive microwave observations.

In addition to evaluating their estimates of snow depth against values from GlobSnow and ERA-Interim/Land, they also use snow density assumptions to estimate snow water equivalent (SWE) for the Northern Hemisphere. Their major conclusion is that SWE has been declining by _5 800 km3 a year, or approximately 139 200 km3 over their 24-year study period. The authors say this decline is equivalent to a 12.5% reduction of SWE over the study period, suggesting the initial amount of SWE was 1113 600 km3.

I believe there is a fundamental flaw in how the authors are calculating annual snow accumulation in this manuscript. Their estimate of annual SWE is orders of magni- tude larger than other global datasets suggest. Mudryk et al. (2015) show that the Northern Hemisphere has an average annual snow accumulation of 3500 km3 (see Figure 1a, taken from Figure 3 in that manuscript). Using four commonly used global datasets (ERA-Interim, GLDAS, MERRA2, and VIC), I estimate the long-term-average global snow storage to be ~4000 km3 (see Figure 1b). Even if these global models/reanalyses are underestimating SWE, it is unlikely they are wrong by as much as this manuscript indicates. I believe the authors may be summing daily values of SWE when calculating their annual total SWE, as one would do when calculating annual precipitation from daily precipitation values. However, this is incorrect when working with SWE. Instead, the authors should consider comparing the annual maximum SWE over their period of record. This will not lead to such a dramatic value of SWE decline, but I think it would be interesting to see how their method compares to changes in SWE from GlobSnow, ERA-Interim/Land, and other global data products.

With this mistake, the manuscript is not ready for publication. But if the authors redo their SWE calculations and the following analyses, I would be interested to see the SWE results from their SVR method. Since this error is critical to the main conclusions of the manuscript, I do not include a review of the rest of the paper.

Reference: Mudryk, L. R., Derksen, C., Kushner, P. J., and Brown, R.: Characterization of Northern Hemisphere Snow Water Equivalent Datasets, 1981–2010, Journal of Climate, 28, 8037-8051.

Response: Thank you very much for your review of our manuscript. We appreciate your positive comments and very useful suggestions for improving the manuscript. We made modification according to your suggestion.

1. The analysis indexes were changed. In Fig. 10, we used annual maximum snow mass, annual average snow mass and annual minimum snow mass to analyze the variation characteristic of snow mass over the past 25 years (1992-2016). The average annual maximum snow mass of NHSnow SWE products have quite same magnitude as the analysis datasets provides by the reviewers and Mudryk et al. (2015), which is approximately 4200 km^3.

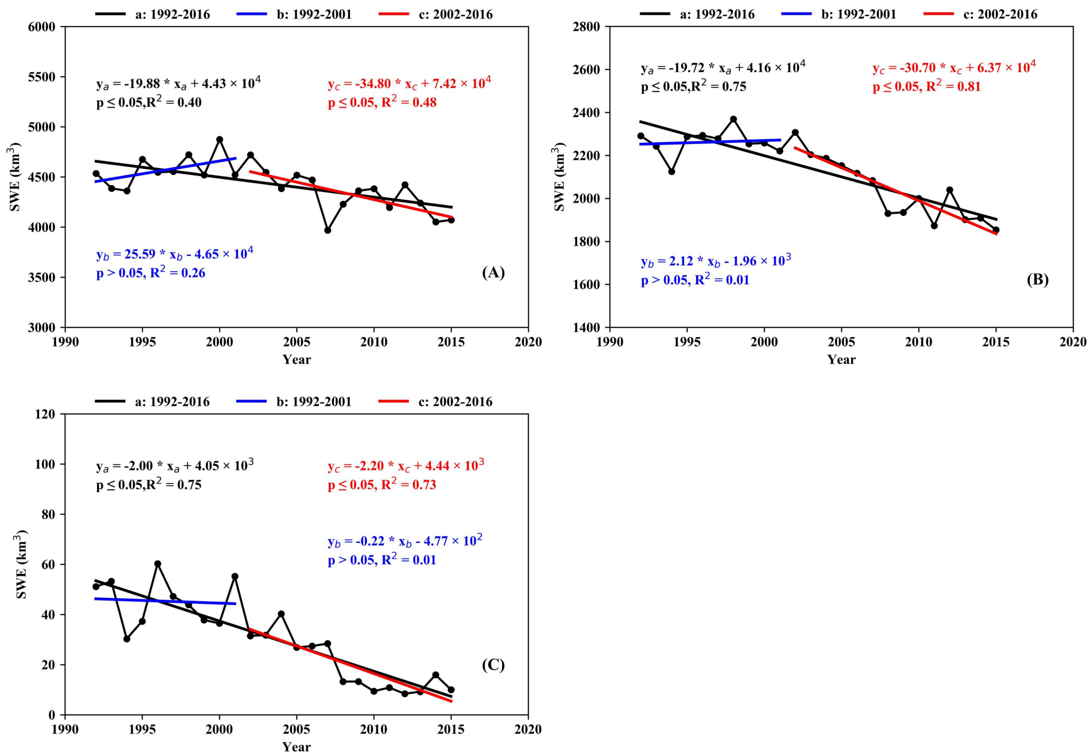

Figure 10. Interannual variation of annual maximum snow mass (A), annual average snow mass (B) and annual minimum snow mass (C) over the Northern Hemisphere for three period 1992-2016 (black line), 1992-2001 (blue line), and 2002-2016 (red line). Trends estimates were computed from least squares. P is the confidence level for the coefficient estimates; R2 is the goodness of fit coefficient.

Subsequently, we mainly revised the description of Paragraph 2 in Section 4.2, the updated description as flowing:

"

The snow mass variation characteristic over the past 25 years were explored by interannual variation (Fig. 10) and intra-annual cycles (not show figure) of snow mass over the Northern Hemisphere . Figure 10 depicts the time series of interannual variation of annual maximum, average and minimum snow mass with respect to 1992–2016 period. The biggest value of annual maximum snow mass occurred in 1998–1999 up to 4875 km^3, while the least was 3969 km^3 in 2007-2008. The annual maximum snow mass present particularly significant decreasing trends ($P \leq 0.05$) during 1992–2016, at the rate of approximately -19.88 km^3 yr.$^{-1}$ (Fig. 10A). Trend analysis

reveals that annual maximum snow mass have a 8% reduction from 1992 to 2016. Note that it present a increase variation trend by about 25.59 km^3 $yr.^{-1}$ ($P > 0.05$) rate for 1992-2001. In contrast, the annual maximum snow mass exhibits a significantly decrease trends (with -34.80 km^3 $yr.^{-1}$, $P \leq 0.05$) since 2002, which would lead to a extraordinary decrease during 1992–2016. According to the static, the annual maximum snow mass usually appear in February (about 60%) and March (about 40%), and in recent several years this occurred in March become a normal state. We can find that the biggest and the least value of annual average snow mass respectively appear in 1998-1999 (~2370 km^3) and 2015-2016 (~1850 km^3) in Fig 10B. Likewise, in Fig 10B and 10C the annual average (minimum) snow mass exhibit a significant decrease trend in 1992-2016 period by rate -19.72 km^3 $yr.^{-1}$, $P > 0.05$ (-2.00 km^3 $yr.^{-1}$, $P \leq 0.05$) and 2002-2016 period at a rate of -30.70 km^3 $yr.^{-1}$, $P > 0.05$ (-2.2 km^3 $yr.^{-1}$, $P \leq 0.05$). For 1992-2016 period, the variation tendency of annual average (minimum) snow mass do not pass the significance level test. Moreover, the reduction for the annual average and annual minimum snow mass is 13% and 67%, respectively.
”

2. We changed the original calculation method of snow mass and only using SWE. The revised Table 7 show the variation of monthly average snow mass.

Table 7. Variation rate and changes of monthly average snow mass during 1992-2016. The asterisk indicate that the changes are significant at 95% confidence level

Month	Variation rate (km^3/yr.)	% Change in the mean of monthly average snow mass
September	-5.96*	-63.89%
October	-25.50*	-43.99%
November	-36.50*	-26.96%
December	-32.66*	-5.00%
January	-34.38*	-9.53%
February	-30.89*	-11.91%
March	1.90	-4.30%
April	-4.29	-6.46%
May	-11.33*	-19.59%
June	-8.01*	-64.67%

We revised the description of Paragraph 3 to flowing statement:
“
When analyzing long-term variation of monthly average snow mass, ten months (September to June) exhibit significant decreasing apart from March and April (Table 7). The maximum decrease rate was approximately -36.50 km^3 $yr.^{-1}$ ($P \leq 0.05$) in November while the minimum decrease occurred in April at -4.29 km^3 $yr.^{-1}$ ($P > 0.05$). An increasing trend appears in March with a rate of approximately 1.90 km^3 $yr.^{-1}$ ($P > 0.05$), however, relatively large decrement in fall and winter are unable to partially be offset by the increment of March. Compared with the fall (September to November) and spring (March to June), the interannual variability of monthly average snow mass significantly decreased in winter (December to February), with average rate of less than -32 km^3 $yr.^{-1}$. The reduction of monthly average snow mass in ten month were generated using the average pattern of each month over 1992-2016 as a reference. We found that the reduction of monthly

average snow mass fluctuated ranging from -65% to -4% for each month (September to June) over 1992-2016 (Table 7). The largest and smallest reduction were about 64.67% and 4.30%, which occurred in June and March, respectively. Variation analysis of monthly average snow mass could offer a powerful evidence for annual average snow mass exhibit a significantly decreasing tendency (Table 7, Fig. 10B).

”

3. We changed (Page 19 Lines 12-15) “Similar conclusions also appear in total SWE change analysis. The total SWE shows a 12.5% reduction and the monthly average total SWE is 65.8% for the largest reduction and a 4.2% for least reduction which occur in June and March, respectively. The total SWE report well-documented significant decreasing trends ($P < 0.05$) during the study period.” to “Similar conclusions also appear in snow mass change analysis. The annual maximum, average and minimum snow mass exhibit significantly decrease trends and respectively show a 8%, 13% and 67% reduction. The monthly average snow mass has shown a decreasing trend almost in every month and the reduction range from 64.67% (June) to 4.3% (March). The annual average snow mass report well-documented significant decreasing trends (~20 km^3 $yr.^{-1}$, $P < 0.05$) during the study period.” in Section 5.

4. In Abstract “Further analysis were performed across the Northern Hemisphere during 1992-2016, which used snow depth, total snow water equivalent (snow mass) and, snow cover days as indexes. Analysis showed the total snow water equivalent has a significant declining trends (~5794 km3 yr.-1, 12.5% reduction)” were revised to “Further analysis were performed across the Northern Hemisphere during 1992-2016, which used snow depth, snow mass and, snow cover days as indexes. Analysis showed annual average snow mass has a significant declining trends (~19.72 km^3 $yr.^{-1}$, 13% reduction).”

Spatiotemporal variation of snow depth in the Northern Hemisphere from 1992 to 2016

Xiongxin Xiao[1, 2], Tingjun Zhang[1, 4], Xinyue Zhong[3], Xiaodong Li[1], Yuxing Li[1]

[1]Key Laboratory of Western China's Environmental Systems (Ministry of Education), College of Earth and Environment Sciences, Lanzhou University, Lanzhou 730000, China

[2]School of Remote Sensing and Information Engineering, Wuhan University, Wuhan 430079, China

[3]Key Laboratory of Remote Sensing of Gansu Province, Cold and Arid Regions Environmental and Engineering Research Institute, Chinese Academy of Sciences, Lanzhou 730000, China

[4]University Corporation for Polar Research, Beijing 100875, China.

Correspondence to: Tingjun Zhang (tjzhang@lzu.edu.cn)

Abstract: Snow cover is an effective best indicator of climate change due to its effect on regional and global surface energy, water balance, hydrology, climate, and ecosystem function. We developed a long term Northern Hemisphere daily snow depth and snow water equivalent product (NHSnow) by the application of the support vector regression (SVR) snow depth retrieval algorithm to historical passive microwave sensors from 1992 to 2016. The accuracies of the snow depth product were evaluated against observed snow depth at meteorological stations along with the other two snow cover products (GlobSnow and ERA-Interim/Land) across the Northern Hemisphere. The evaluation results showed that NHSnow performs generally well with relatively high accuracy. Further analysis were performed across the Northern Hemisphere during 1992-2016, which used snow depth, snow mass and, snow cover days as indexes. Analysis showed annual average ~~the~~ snow mass has a significant declining trends (~19.72 km^3 $yr.^{-1}$, 13% reduction) ~~(~5794 km^3 $yr.^{-1}$, 12.5% reduction)~~. Although spatial variation pattern of snow depth and snow cover days exhibited slight regional differences, it generally reveals a decreasing trend over most of the Northern Hemisphere. Our work provides evidence that rapid changes in snow depth and snow water equivalent are occurring beginning at the turn of the 21st century with dramatic, surface-based warming.

1. Introduction

Seasonal snow cover is an important component of the climate system and global water cycle that stores large amounts of freshwater and play major impacts on the surface energy budget, climatology and water management (Immerzeel et al., 2010;Zhang, 2005;Robinson and Frei, 2000;Tedesco et al., 2014). On account of the high albedo and low heat conductivity properties of snow, snow cover may directly modulate the land surface energy balance (Flanner et al., 2011), influence on soil thermal regime (Zhang et al., 1996;Zhang, 2005), and indirectly affect atmospheric circulation (Cohen et al., 2012;Zhang et al., 2004;Li et al., 2018). Most jurisdictions in the Northern Hemisphere rely on natural water storage provided by snowpack (Diffenbaugh et al., 2013;Barnett et al., 2005), supplying water for domestic and industrial use (Sturm, 2015;Qin et al., 2006). Accurate estimation of and reliable information on snow cover spatial and temporal change at regional and global scales is very critical for climate change monitoring, model evaluation and water source management (Brown and Frei, 2007;Flanner et al., 2011).

Snow depth (SD) is most commonly measured using in situ observations. Given the sparseness of measurements, it is not possible to fully capture spatial variability of snow cover. Although the in situ observation method is accurate, it is unrealistic in mountain regions and low population zones because it is labor, material and financial resource intensive. Remote sensing is the most effective and powerful way of obtaining information of snow cover over larger areas (Foster et al., 2011). Optical remote sensing is capable of observing large areas of snow; however, it is unable to observe the Earth's surface under cloudy conditions (Foster et al., 2011;Che et al., 2016;Dai et al., 2017). However, microwave remote sensing has this potential and is an attractive alternative to optical remote sensing under all weather conditions and round the clock. It can also be used to estimate SD and snow water equivalent (SWE) due to the interaction with snowpack by providing dual polarization data at different frequencies (Chang et al., 1987;Che et al., 2008;Takala et al., 2011).

Snow cover products derived from passive microwave (PM) data have been widely applied to investigate regional and global climate change, and validate hydrological and climate models (Brown et al., 2010;Brown and Robinson, 2011;Dai et al., 2017). Progress in satellite data acquisition, as well as SD/SWE retrieval algorithm development, have led to a global improvement in snow monitoring (Qin et al., 2006;Snauffer et al., 2016). The PM brightness temperature of the SMMR (Scanning Multichannel Microwave Radiometer), SSM/I (Special Sensor Microwave Imager), AMSR-E (Advanced Microwave Scanning Radiometer for Earth Observing System), AMSR2 (Advanced Microwave Scanning Radiometer 2 on the Global Change Observation Mission – Water), SSMIS (Special Sensor Microwave Imager), SSM/I (Special Sensor Microwave Imager Sounder) and, FY-3B/C (Fengyun-3 satellite B/C) are available and several algorithms have been developed to estimate SD and SWE using PM brightness temperature data (Chang et al., 1987;Dai et al., 2012;Xiao et al., 2018;Pulliainen, 2006;Takala et al., 2011;Che et al., 2008;Foster et al., 1997).

Most retrieval algorithms operate on the principle that the difference in brightness temperature between 18 and 37 GHz reflects the quantity of SD and SWE (Chang et al., 1987). Over and underestimated trends are prevalent in these linear SD and SWE retrieval algorithms (Gan et al., 2013) for which there are two possible and reasonable explanations. One is that vegetation overlaying snow attenuates its microwave scatter signal and results in underestimating SD and SWE from PM data (Che et al., 2016;Vander Jagt et al., 2013). To reduce the effect of tree canopy, a forest fraction was introduced into retrieval algorithm developed to estimate SD and SWE (Foster et al., 1997;Che et al., 2008), or the retrieval algorithm was constructed based on particular land cover types (Goïta et al., 2003;Che et al., 2016;Derksen et al., 2005;Foster et al., 2009). The other explanation is that the relationship between snow properties (SD or SWE) and the PM brightness temperature is non-linear. Newer approaches (e.g. artificial neural networks, support vector regression, decision tree) have emerged using data-mining and have been explored to retrieve SD and SWE that are intended to replace traditional linear methods (Gharaei-Manesh et al., 2016;Tedesco et al., 2004;Liang et al., 2015;Forman et al., 2013;Xue and Forman, 2015). However, there are remain some limitations for these retrieval algorithms due to the diversity of land cover types and the spatiotemporal heterogeneity of snow physical properties.

Numerous studies have reported the changes in snow cover extent (SCE) at regional and hemispheric scales (Rupp et al., 2013;Dai et al., 2017;Derksen and Brown, 2012;Brown and Robinson, 2011;Huang et al., 2016). Huang et al. (2017) repored the impact of climate and elevaion on snow cover varition in Tibetan Plateau, including SWE, snow cover area and, snow cover days. Hori et al. (2017) developed a 38-year Northern Hemisphere daily snow cover extent product and analyzed seasonal Northern Heimsphere snow cover extent variation trends. In this study, SD was selected as basis for analyzing spatiotemporal change of snow cover. SD provides an additional dimension to snow cover characteristics. Barrett et al. (2015) explored intra-seasonal variability in springtime Northern Hemisphere daily SD change by the phase of the Madden–Julian oscillation. Wegmann et al. (2017) compared four long-term reanalysis datasets with Russian SD observation data. However, this study only focused on snowfall season (October and November) and snowmelt season (April). SD change trends have also been analyzed at regional scales (Ye et al., 1998;Dyer and Mote, 2006). Several studies quantified the spatial and temporal changes consistency of SWE or snow mass derived from satellite data (Mudryk et al., 2015) but these studies have focused on the limited dimension of snow cover variation. Dyer and Mote used a gridded dataset to study regional and temporal variability of SD trends across North America from 1960-2000 (Dyer and Mote, 2006) and the characteristic of seasonal snow extent and snow mass in South America form 1979 to 2006 was descripted and reported (Foster et al., 2009).

There are, however, very limited data (station data, satellite data or otherwise) that can provide both SD and SWE on a hemispheric scale. This paper describes the approach to develop a consistent 25-year of daily SD and SWE of Northern Hemisphere utilized multi-source data. The primary objective of this study is to develop 25 years (1992-2016) hemispherical SD and SWE product (hereafter referred to as the NHSnow) with a 25 km spatial resolution using SVR SD retrieval algorithm. This paper will address the following questions: 1) How consistent are NHSnow and other sourced snow cover datasets with the in situ SD observation? 2) What is the spatiotemporal variability of snow cover in the Northern Hemisphere from 1992-2016? Meanwhile, it is extremely challenging to make extensive quantitative validation of SD and SWE estimates.

This paper is organized in five sections, as follows. Section 2 describes the data sets used in this study. The methods of data preprocessing and snow cover products generation were provided in Section 3. Next, we describe NHSnow validation against in-situ snow observation record, exhibit the variability of snow cover in the Northern Hemisphere and discuss the potential effect factors for the variation results utilized NHSnow data (Section 4). Finally, section 5 summarizes the work of this paper.

2 Datasets

2.1 Passive microwave data

Because cloud often appear in the snow cover region or condition, during the winter season often conceals snowfall possibility, here is particularly advantageous using passive microwave remote sensing. SSM/I and SSMIS is PM radiometer onboard United States Defense Meteorological Satellites Program (DMSP) satellite (available from the National Snow and Ice Data Center, http://nsidc.org/data/NSIDC-0032). The SSM/I (F11 and F13) dataset from this platform, as well as

SSMIS (F17), present with the equal-area scale earth grid (EASE-Grid) format and 25 km spatial resolution (Brodzik and Knowles, 2002;Armstrong, 2008;Wentz, 2013;Armstrong and Brodzik, 1995) (Table 1). The snow cover area and SD derived from SSM/I (F11) and SSM/I (F13) data have high consistency rendering the calibration between these two sensors for snow cover area and SD unnecessary (Dai et al., 2015). To minimize the melt-water effect to some extent, which can change the microwave emissivity of snow, only descending orbit (nighttime) passive microwave data were used (Foster et al., 2009).

2.2 Ground-based data

Ground SD observation are used to construct and verify the SD retrieval model in this study from two sources of daily SD observation. The first is the Global Surface Summary of the Day (GSOD) dataset provided by National Oceanic and Atmospheric Administration (NOAA) (https://data.noaa.gov/dataset/dataset/global-surface-summary-of-the-day-gsod). This online dataset, which began in 1929, is derived from the Integrated Surface Hourly (ISH) dataset (Xu et al., 2016). There are fourteen daily elements in GSOD dataset, including SD measured at 0.1 inch. The missing of SD or reported 0 on the day would be marked 999.9. Data at approximately 30000 meteorological stations were recorded of which 9000 typically are valid. In our study period and area, more than 17 000 meteorological station were selected with records from 1991 and a location far from large water bodies.

To supplement data from stations that were not reporting during the study periods, ground-based measurements of daily SD were gathered from an additional 635 Chinese meteorological stations available at the National Meteorological Information of China Meteorological Administration (Xiao et al., 2018;Zhong, 2014). These daily SD records begun in 1957 include SD (unit, cm), observation time, and geographical location information available (http://data.cma.cn/en).

2.3 Topographic and land cover data

We also used topography as an auxiliary information to estimate SD (Xiao et al., 2018). Elevation was available from ETOPO1 at a resolution of 1 arc-minute (Amante, 2009) available at (http://www.ngdc.noaa.gov/mgg/global/). To match the resolution of the PM brightness temperature data with 25 km spatial resolution, we resampled the ETOPO1 to 25 km resolution (Fig. 1).

To increase the accuracy of SD estimates for different land cover types, we both used MODIS land cover (MCD12Q1 V051) from 2001 to 2013 (Friedl and Sulla-Menashe, 2011;Friedl et al., 2010) and Advanced Very High Resolution Radiometer (AVHRR) Global Land Cover classification generated by the University of Maryland Department of Geography. The MCD12Q1 International Geosphere-Biosphere Program (IGBP) classification scheme divides land surface into 17 types, which were reclassified into five classes according to Xiao et al (2018) study.

AVHRR imagery was acquired between 1981-1994 from the NOAA-15 satellite (Hansen et al., 2000) and were categorized into fourteen land cover classes at 1 km resolution. These data allowed us to adjust the proposed snow-depth retrieval algorithm by reclassifying the fourteen native land cover classes into five classes (water, forest, shrub, prairie and, bare-land) at 25 km spatial resolution (Table A.). MCD12Q1 is available at site https://earthdata.nasa.gov/, while AVHRR land cover data is available from http://www.landcover.org/data/landcover/.

2.4 Satellite snow cover datasets

Two kinds of snow cover datasets were utilized based on two criteria: covering the Northern Hemisphere and long-term availability. We selected GlobSnow and ERA-Interim/Land which are widely used in global and regional climate change studies (Snauffer et al., 2016;Hancock et al., 2013;Mudryk et al., 2015). These datasets were used to compare with the NHSnow SD product.

In November 2013, the European Space Agency (ESA) released the GlobSnow Version 2.0 SWE and Snow Extent (SE) data for the Northern Hemisphere (Takala et al., 2011;Pulliainen, 2006). These data include all non-mountainous areas in the Northern Hemisphere and are available online (http://www.globsnow.info/). Processing includes data assimilation based on combining satellite PM remote sensing data (SMMR, SSM/I and SSMIS), spanning December 1979 to May 2016, with ground-based observation data in a data assimilation scheme to derive SWE. GlobSnow Version 2.0 (hereinafter referred as GlobSnow) provides three kinds of temporal aggregation level products with 25 km spatial resolution: daily, weekly and monthly. This dataset covers all land surface areas in a band between 35° N ~ 85° N excluding mountainous regions, glaciers and Greenland. To convert between SD and SWE using GlobSnow, the snow density is held constant at 0.24 g/cm^3 (Sturm et al., 2010;Hancock et al., 2013;Che et al., 2016).

ERA-Interim/Land (Balsamo et al., 2015) is a global land-surface reanalysis product with data from January 1979 to December 2010 based on ERA-Interim meteorological forcing. It is produced by a land-surface model simulation using the Hydrology Tiled ECMWF Scheme of Surface Exchange over Land (HTESSEL), with meteorological forcing from ERA-Interim. Dutra et al. (2010) described the snow scheme and demonstrated the verification using field experiments. “SD”, which actually is SWE, is one of the thirteen parameters provided. We should convert SWE to SD using the associated snow density data. These two datasets are available online (http://apps.ecmwf.int/datasets/data/interim-land/type=an/). To maximum the proximity to the descending orbit time of passive microwave sensor, the data with analysis type at 6 o’clock were used in this study, and the spatial resolution of these data is 0.125 degree.

2.5 Snow classification data

In order to accurately estimate SWE, snow classification data were used to convert SD into SWE. Global Seasonal Snow Classification System was defined by Sturm et al. (1995) based on snow physical properties (SD, thermal conductivity, snow density snow layers, degree of wetting, etc.), and seasonal snow cover. Snow cover were categorized into six snow classes (tundra, taiga, alpine, maritime, prairie, and ephemeral) plus water and ice fields (Figure 2). Snow classification data can be accessed from the National Center for Atmospheric Research (NCAR)/Earth Observing Laboratory (EOL) (https://data.eol.ucar.edu/dataset/6808). The snow classification dataset was developed and tested for the Northern Hemisphere at 0.5-degree spatial resolution(Sturm et al., 1995).

3 Methods

3.1 Theoretical basis

Snow distribution is affected by various factors, but not limited to, vegetation (Che et al., 2016;Vander Jagt et al., 2013), soil and air temperature (Forman and Reichle, 2015;Grippa et al., 2004;Dai et al., 2017), topography and wind (Smith and Bookhagen, 2016). The snow retrieval process uses DS and other parameters (A, T, G, L, D ...) to yield snow parameters (e.g. SD, Eq. 1) (Xiao et al., 2018).

$$[S] = g\,(A, T, G, L, DS, D\ ...) + \varepsilon \tag{1}$$

where g (·) denotes the retrieval function. DS is the digital signal from remote sensing sensor (PM, active microwave, visible spectral remote sensing etc.), A is the atmosphere (wind speed, air temperature, humidity, precipitation etc.), T is the topography (latitude, longitude, elevation, terrain slope, aspect etc.), L is the location (latitude, longitude), G is the ground (ground surface temperature, vegetation type etc.), S is the snow properties (snow grain size, density, reflectance, SD, SWE etc.), D is the day of year and ε is the residual error or uncertainty that describes the relationship between sensor signal and measured snow properties.

The SVR SD retrieval algorithm also follows the snow retrieval process (Eq. 1). We utilized ten parameters were as input parameters, including PM brightness temperature (19 GHz, 37 GHz, 85 GHz, or 91 GHz) with vertical and horizontal polarizations, geophysical location (latitude and longitude), elevation and, the measured SD. The output parameter is the estimated SD. Apart from above factors, the SVR SD retrieval algorithm also considers other influence factors, including wet snow, land cover types and day of year (Xiao et al., 2018) to improve the accuracy of estimated SD. Day of year have been converted into three snow cover stages, which mean indirectly considering snow properties evolution.

3.2 Processing flow overview

The SVR SD retrieval algorithm first proposed by Xiao et al. (2018), which indirectly considers seasonal variation and vegetation influence in the evolution of snow properties, was used to estimate SD. In Eurasia, it was found that the SVR SD retrieval algorithm performs much superior with reduced uncertainties compared based upon the correlation coefficient (R), mean absolute error (MAE), and root mean squared error in Xiao et al. (2018) study. It should be noted that this study used daily observation in the Northern Hemisphere with exception of July and August. Here, we provide more detailed but different descriptions for the SVR SD retrieval algorithm in several steps (Fig. 3). The detailed descriptions of the other steps can refer to the Xiao et al paper (Xiao et al., 2018) not repeated here.

Step 3. Due to our study period pre-dates MODIS data, we used AVHRR land cover as suppliment data. MODIS and AVHRR land cover were reclassified into four classes (forest, prairie, shrub and bare-land) which were bases of construting SD retrieval sub-model. Table A (in appendix) describes the reclassification scheme of AVHRR land cover is described. MODIS land cover reclassification schemes were documented in Xiao et al. (2018). Because of the relative stability of land cover change, MODIS land cover in 2013 was used for each year during 2013–2016. Similarly, MODIS land cover in 2001 was used in each year during 1998–2001, and AVHRR land cover data were used for 6 years (1992–1997).

Step 6.1 Construction of a subcontinental model. It needs to be stressed that the snow properties in the Eurasia (EU) and North America (NA) exhibit noticed discrepancy especially in snow density. (Zhong et al., 2014;Bilello, 1984). One study pointed out that mean snow density in the former Soviet Union (0.21 ~ 0.31 g/cm^3) was lower than the data from NA (0.24 ~ 0.31 g/cm^3) (Bilello, 1984), and also Zhong et al. (2014) explained the possible reasons which resulting in the diversity of snow density in EU and NA. Based on this, we separately constructed the SD retrieval models for EU and NA.

Step 6.2 Training dataset selection is the process of removing redundant features from spatial data. The accuracy of estimated SD primarily depends on training data quality, which also demonstrate the significance of the selection rule of training samples (Xiao et al., 2018). Inputting more data than needed in the training dataset to train SD retrieval model, may lead to overfitting and an estimated SD with high error. In this study, we collected an extremely large number of daily SD records over 25 years, necessitating a optimized selection rule to avoid data information redundancy.

The selection rule proposed in previous research (Xiao et al., 2018) was modified and then it was divided into two steps in here. Firstly, the numbers of sample in the three layers, layer1 ($0 \leq SD < 50$), layer2 ($50 \leq SD < 100$) and layer3 ($SD \geq 100$), should be concretely quantified. To aviod an inflated training sample in layer2 and layer3, we set a threshold (3 000) determined by several tests (not shown). A threshold (12000) for layer1 was adopted following Xiao et al. (2018). Table 2 descriped the section of training sample for each layer in detail. After that, the quality of training sample in each layers determined by stratified random sampling is the second step. Stratification was performed in 1 cm SD intervals. Note that, all the selecton operations in here were randomly performed.

Step 7. Through above steps, the daily estimated SD data in the Northern Hemisphere from January 1992 to December 2016 (excluding July and August) were obtained. Owning to the nature of radiometer observations, NHSnow products are only reliable in areas with seasonal dry snow cover. Areas with sporadic wet or thin snow are not reliably detected and areas marked as snow-free may include areas with wet snow. If one pixel is detected as snow cover by the detection decision tree (Grody and Basist, 1996), but is likely to be shallow or medium-to-deep snow with an estimated value of equal or less than 1 cm, the SD value is set as 5 cm (Che et al., 2016;Wang et al., 2008) (Fig. 4.).

Step 8. In this study, Greenland and Iceland are excluded from the generation and analysis of NHSnow (NH_SD, NH_SWE) products due to their complex coastal topography and the difficulty in discriminating snow from ice (Fig. 4) (Brown et al., 2010). Missing data and zero-data gaps occur in the process of generating daily SD gridded products. Therefore, the following filters were applied. Daily estimated SD was averaged with a sliding 7-day window to reduce noise and compensate for missing data in the daily time series. For example, the SD estimate for 4 January is an average of the assimilated scheme output for 1 to 7 January (Takala et al., 2011;Che et al., 2016). When finished, the sliding SD method generated daily SD products for the entire Northern Hemisphere (NH_SD; Fig. 4).

3.3 Estimation of SWE

SWE contains more useful information for hydrologists than SD because it represents the amount of liquid water in the snowpack available to the ecosystem as the snow melts. One way to estimate SWE uses SD and snow density (ρ) as described in Eq. 2. Northern Hemisphere SWE products were generated in this study using snow density that converts SD to SWE. (Eq. 2, Fig. 3 and 4, Step 9).

$$\mathrm{SWE}(mm) = \mathrm{SD}(cm) \times \rho(g/cm^3) \times 10 \tag{2}$$

At present, the primary problem is to obtain relatively accurate snow density. In this study, dynamical calculation methods were adopted to estimate snow density. Two methods are usually used to convert SD to SWE. The first uses a fixed value, 0.24 g/cm^3 (or other value), without spatiotemporal variation (Che et al., 2016;Takala et al., 2011). The second uses a temporally static by spatially variable mask of snow density to estimate SWE and are used to generate current AMSR-E SWE products (Tedesco and Narvekar, 2010). Since the snowpack are usually rather unstable, it is awfully unreasonable to set the snow density in the whole snow season to a constant. Observations show that snow density does evolve and tends to increase (decrease) throughout the snow season (from September to June) (Dai et al., 2012;Sturm et al., 1995). Here, daily snow density is obtained following Sturm et al.(2010) (Eq. 3).They used daily SD, day of the year (DOY), and the snow climate class (SC) to produce snowpack bulk density estimates. In this method, knowledge of SC is used to capture field environment variables (air temperature, initial density) that have a considerable effect on snow density evolution.

$$\rho(\mathrm{SD,DOY,SC}) = (\rho_{max} - \rho_0)[1 - exp(-k_1 \times SD - k_2 \times DOY)] + \rho_0 \tag{3}$$

where ρ_{max} is the maximum density, ρ_0 is the initial density, k_1 and k_2 are densification parameters for SD and DOY, respectively. k_1, k_2, ρ_{max}, ρ_0 vary with SC (Table 3). For operational purposes in our work, DOY extend to 1 September each year (Matthew Sturm, personal communication, 2018) running from −122 (1 September) to 181 (30 June). Sturm et al. (2010) didn't compute snow density for the SC as ephemeral snow despite its presence in the Northern Hemisphere. According to Zhong et al. (2014) study, the snow density of ephemeral is set to an fixed value, 0.25 g/cm^3. Finally, daily snow density is simulated by the Eq. 3 in the Northern Hemisphere during the 1992−2016 period.

4 Results and Discussion

4.1 Snow depth

4.1.1 Validation of snow depth

Here to give insight into relative performance of SD products, we compared three sources of snow cover product (NHSnow, GlobSnow, and ERA-Interim/Land) with ground SD observations (Fig. 5-7) using three indices bias, mean absolute error (MAE) and root mean square error (RMSE).The common period (1992 - 2010) daily SD of three products (Section 2.4) were collected as validation data. This validation work primarily focus on snow cover stabilization stage (December to February). Since the snow density change slowly over a smaller range in snow cover stabilization stage (Xiao et al., 2018), using a constant value (0.24 g/cm^3) for GlobSnow could introduce relative little error (Section 3.3). Subject to the unavailability of SWE station observations, the evaluation of SWE can't be carried out.

The relatively little bias (blue and green dots) between the estimated SD from three products against measured SD is located in mid and low latitude regions (< 60 °N) for these three snow depth datasets (NHSnow, GlobSnow, and ERA-Interim/Land; Fig. 5). However, a large bias was found in the polar region and along the coast, such as the north of Russia near the Arctic Ocean, Russian Far East, Korean peninsula, Northern Mediterranean and Northeast Canada. For NHSnow and GlobSnow, most bias is distributed near the μ=0 line with high frequency, although some bias is greater than 100 (or less than −100) (Fig. 5b, d). Positive (negative) biases indicate mean grid cell values less (greater) than those of the respective stations SD measures. Fig. 5c showed the ERA-Interim/Land overestimate snow depth in Western Siberian Plains and Eastern European Plains (around 60 °N; orange dots). As reference, Average SD pattern of three products in February (1992-2010) were also provided in Appendix (Fig. A)

For analysis indexes, MAE and RMSE, the distribution of error points of NHSnow and GlobSnow are much the same as the distribution of its bias (Fig. 5-7).We used all evaluation records to calculate three precision indexes for three products. We found that the bias, MAE and RMSE is 0.59 cm, 15.12 cm and 20.11 cm, respectively, for NHSnow gridded product, but more bias (1.19 cm), MAE (15.98 cm) and lower RMSE (15.48 cm) for GlobSnow (Table 4). This comparison (NHSnow vs. GlobSnow) showed relatively good agreement, although NHSnow over- or underestimated the SD with larger RMSE. Overall, the performance of GlobSnow was better than the NHSnow gridded product. However, part of the validation data were also applied for GlobSnow assimilation, it is highly possible that in this case GlobSnow validation may not completely independent. The different performance for these two products may be mainly because the evolution of snow grain size by HUT (The Helsinki University of Technology) model was used to generate SWE in GlobSnow. Che et al. (2016) reported that the grain size is more important than snow density and temperature. Further, ERA-Interim/Land had the worst performance of all three products with highest bias (-5.60), MAE (18.72) and RMSE (37.77). The smallest bias is located near mid-latitude regions (< 50 °N) and much of the bias lies at 0–100 cm for ERA-Interim/Land products (Fig. 5e, f). It must be noted that there are 89 bias records in two stations, which located in Novosibirsk Islands and Victoria Island, is much less than -300 cm (approximately -3000 cm). Large MAE and RMSE can be found in high latitude and coastal region (Fig. 5e). Unlike NHSnow and GlobSnow, ERA-Interim/Land is more likely to overestimate SD and appears to be less consistent with in situ observation across the Northern Hemisphere (Fig. 5f). Through analyzing ground observation, we can see that deep snow is distributed in high latitude areas.

While the gridded products do a fairly good job of representing smaller accumulations of SD (shadow and mid-deep snow cover), they all struggle to capture very high accumulations (deep snow) with less bias, MAE and RMSE (Fig. 5-7, Fig. A). As a result, variation in snow cover could fail to be adequately captured in areas with frequent deep snow and, thus, we should be cautious when interpreting of this validation result.

Uncertainties in these three gridded snow products caused by ground temperature and topographic factor could result in some level discrepancies between the measured and the estimated SD (Vander Jagt et al., 2013;Snauffer et al., 2016). Forests exhibit strong influence on snow distributions by canopy interception and the evolution of snow properties. The dense portions of boreal forests are widely distributed in NA and northern EU (Friedl et al., 2010) Large bias, MAE and RMSE regions of three gridded products (Fig. 5-7) cover vast areas of tall vegetation (forests and shrub). Furthermore, the spatial inhomogeneity cause one grid cells (~25 km) that is almost not possible to completely cover by one vegetation type (low heterogeneity). Because the estimated SD of NHSnow depends on land cover types, this discrepancy induced by surface cover heterogeneity could partly account for why NHSnow has a smaller MAE and RMSE for low vegetation (bare-land and prairie) distributed at middle and low latitudes, than the higher vegetation (shrub and forest) areas at higher latitudes (Xiao et al., 2018).

As well, there are scale mismatches between in situ observation and the gridded products with regard to snowpack properties and their spatiotemporal representativeness (Frei et al., 2012). It is difficult to precisely validate coarse-resolution satellite observation using ground truth. Subsequently, over- or underestimates are inevitable when using a single in situ (SD or SWE) observation to test the veracity of the gridded products (Mudryk et al., 2015;Xiao et al., 2018). Snow surveys would benefit from multiple measurements at different points within one pixel (López-Moreno et al., 2011). In situ observations are highly representative when the SD varies smoothly in space, and poorly representative when the SD is spatially stepped (Che et al., 2016). However, there is almost always a lack of sufficient ground-measured data. To date, field site observations are still to be more authentic and reliable datasets than satellite observation.

As a whole, the accuracy of estimated SD in the Northern Hemisphere presented a spatial heterogeneity. Issues of scale and spatial heterogeneity of validation data notwithstanding, these comparisons conducted in our work can yield valuable insight into the performance of these products.

4.1.2 Variation of snow depth

To better understand and interpret snow cover variation across the Northern Hemisphere, we conducted an analysis of SD variation using seasonal maximum SD from 1992–2016. According to the rules of variation level grading, which was divided into 5 grade (extremely significant increase, significant increase, non-significant change, extremely significant decrease, and significant decrease; Table 5), we can easily gained seasonal maximum SD variation level range 1992 to 2016. Figure 8 shows the variation pattern of seasonal maximum SD in three seasons (fall, winter and spring) with statistical significance level. In three seasons, variation trend of seasonal maximum SD exhibited a distinctly different pattern over the Northern Hemisphere since 1992. Seasonal maximum SD variation results in fall illustrated that a reduction trend account for most area of the EU with the rate ranging from 0 to 1 cm yr.$^{-1}$. The Figure 8a show the significant level pattern of corresponding maximum SD change trend. We can find that the area, which show extremely significant decrease in fall, are mainly located in the Russian Far East, the Qinghai-Tibet Plateau, the southern Siberian Plateau, and the northeastern region of Canada. On the contrary, Russia's Taimer Peninsula and the United States' Alaska region shows extremely significant increase trend (0 ~1 cm yr.$^{-1}$). In addition, the maximum SD in winter and spring also exhibited extremely significant decrease in the Qinghai-Tibet Plateau and the northeastern region of Canada as shown in Figure 8b and 8c. The area with extremely significant decrease trend extent add a Western Siberian plain region. Wang and Li (2012) used nearly 50a of daily station SD observation data to analyze the trend of maximum SD in China. The variation trend of seasonal maximum SD in the Qinghai-Tibet Plateau form previous study is consistent with the conclusion observed in this study (Wang and Li, 2012).There are more regions in seasonal maximum SD with extremely significant increase trend in winter and spring (green region). Furthermore, a strange phenomenon that the variation trend of seasonal maximum SD in the Russian Far East show extremely significant decrease, while it is in inverse in spring. This variation trend of maximum SD in spring analyzed using NHSnow products is consistent with the analysis results using GlobSnow products from recently published study (Wu et al., 2018). It need be pointed out that the significant increase (decrease) area is located around extremely significant increase (decrease) as shown in Figure 8. No matter which season, although the variation trend of maximum seasonal SD didn't pass the significance level test, we can draw the conclusion that the wide range of area across the Northern Hemisphere experienced pronounced change during the period 1992 to 2016.

Finally, we analyzed season variation analysis of SD across the Northern Hemisphere using seasonal average SD as analysis index. Seasonal average SD was defined as the cumulative SD divided by the days in one snow cover season.SD variation rate fluctuated in different regions and seasons. It was generally large in the region north of 55° N (Fig. 9, Fig. B and C in appendix). This fluctuation was large in winter with high of -0.11 ± 0.40 cm yr.$^{-1}$ than other seasons during 1992–2016 (Fig. 9d, Table 6.), which means that the maximum changes occurred in winter. Similar conclusion also can be easily found in the two periods 1992–2001 and 2002–2016 (Fig. B-d, C-d and Table 6). Although not all variation trends passed the significance test, most regions in the Northern Hemisphere show increasing trends during 1992-2001 (Fig. B; Table 6). The SD variation trend in the three seasons during 2002–2016 was reversed. The SD absolute variation rate during 2002–2016 is apparently greater than its rate during 1992–2001 (Fig. C; Table 6). The last century were considered to be the warmest period.

The high fluctuation of SD variation rate especially occurred in the polar region (the arctic and the Tibetan plateau) for three seasons. In the context of global climate change, we found that winter SD variation was more sensitive to climate change (Brown et al., 2010). The strength of this relationship is spatially complex, varying by latitude, region, and climate condition.

4.2 Snow mass

GlobSnow dataset covers all land surface areas excluding mountainous regions, glaciers and Greenland as described in Section 2.4. From above analysis, we can find that ERA-Interim/Land have somewhat poor performance in SD estimation. Thus, further analysis of snow cover variation in the Northern Hemisphere used NHSnow products as analysis data. The forecast for snow mass have great potential consequences on agriculture practices in many regions. Snow mass in here is calculated by SWE multiplied by snow cover area (Qin et al., 2006). It should be noted that the snow classification tree (Grody and Basist, 1996), which have been applied in many studies (Che et al., 2008;Dai et al., 2017;Yu et al., 2012), was used to detect snow cover for NHSnow product. Liu et al. (2018) also reported that Grody's algorithm had higher positive predictive values and lower omission errors by testing snow cover mapping algorithms with the in situ SD over China. In this study, Annual~~ (or monthly~~) average (maximum, and minimum) in one snow cover year (excluded July and August) were calculated as analysis indexes and also monthly average snow mass in 25 years~~, which is the sum of daily (or the mean of monthly) total SWE in one snow cover year (or each month of 25 years)~~.

The snow mass variation characteristic over the past 25 years were explored by i~~I~~nterannual variation (Fig. 10) and intra-annual cycles (not show figure) of ~~total SWE~~snow mass over the Northern Hemisphere ~~were used to analyze total SWE variation characteristic over the past 25 years (1992–2016)~~. Figure 10~~8~~ depicts the time series of interannual variation of annual ~~total SWE~~maximum, average and minimum snow mass ~~anomaly~~ with respect to 1992–2016 ~~reference~~ period. The biggest value of annual maximum snow mass ~~anomaly~~ occurred in 1998–1999 up to 4875 km^3 ~~period~~, ~~with~~ while the least ~~minimum~~ was 3969 km^3 in ~~during~~ 2007-2008~~2015–2016~~. ~~It~~ The annual maximum snow mass present particularly significant decreasing trends ($P \leq 0.05$) during 1992–2016, at the rate of approximately -~~5794~~ 19.88 km^3 yr.$^{-1}$ (Fig. 10A). Trend analysis reveals that annual maximum ~~total SWE~~snow mass have a 8~~12.5~~% reduction from 1992 to 2016. Note that it~~There~~ ~~is~~ present a ~~slow~~ increase variation trend ~~rate~~ by about ~~710~~ 25.59 km^3 yr.$^{-1}$ ($P > 0.05$) rate for 1992-2001~~ period~~. In contrast, the annual maximum ~~total SWE~~snow mass exhibits a ~~anomaly~~ significantly decrease trends (with -34.80 km^3 yr.$^{-1}$, $P \leq 0.05$) ~~after~~ since 2002~~ at rate of approximately~~ ~~-9041 km^3 yr.$^{-1}$~~, which ~~may~~ would lead to a extraordinary decrease~~ing~~ ~~trends of total SWE~~ during 1992–2016. According to the static, the annual maximum snow mass usually appear in February (about 60%) and March (about 40%), and in recent several years this occurred in March become a normal state~~There was a sudden drop of total SWE in 2008–2009 as found in previous studies~~. We can find that the biggest and the least value of annual average snow mass respectively appear in 1998-1999 (~2370 km^3) and 2015-2016 (~1850 km^3) in Fig 10B. Likewise, in Fig 10B and 10C the annual average (minimum) snow mass exhibit a significant decrease trend in 1992-2016 period by rate -19.72 km^3 yr.$^{-1}$, $P > 0.05$ (-2.00 km^3 yr.$^{-1}$, $P \leq 0.05$) and 2002-2016 period at a rate of -30.70 km^3 yr.$^{-1}$, $P > 0.05$ (-2.2 km^3 yr.$^{-1}$, $P \leq 0.05$). For 1992-2016 period, the variation tendency of annual average (minimum) snow mass do not pass the significance level test. Moreover, the reduction for the annual average and annual minimum snow mass is 13% and 67%, respectively. ~~However, o~~Other factors, for instance, oceanic and atmospheric heat transport, sea ice season wind, and solar insolation anomalies, may have contributed to the fluctuation of ~~total SWE~~snow mass (Liu and Key, 2014). Variation of ~~total SWE~~snow mass across the Northern Hemisphere could well capture the variation characteristic of the Arctic sea ice extent (Tilling et al., 2015).

When analyzing long-term variation of monthly average ~~total SWE~~snow mass, ten months (September to June) exhibit significant decreasing apart from March and April (Table 7). The maximum decrease rate was approximately -~~1066~~ 36.50 km^3 yr.$^{-1}$ ($P \leq 0.05$) in ~~January~~ November while the minimum decrease occurred in ~~September~~ April at -4.29~~177~~ km^3 yr.$^{-1}$ ($P > 0.05$). An increasing trend appears in March with a rate of approximately 1.90~~68~~ km^3 yr.$^{-1}$ ($P > 0.05$), however, relatively large decrement in fall and winter are unable to partially be offset by the increment of March. Compared with the fall (September to November) and spring (~~February~~ March to June), the interannual variability of monthly average ~~total SWE~~snow mass significantly decreased in winter

(December to ~~January~~February), with average rate of less than -32~~1000~~ km^3 yr.$^{-1}$. The reduction of monthly average snow mass in ten month were generated using the average pattern of each month over 1992-2016 as a reference. We ~~also~~ found that the reduction of monthly average ~~total SWE~~snow mass ~~reduction~~ fluctuated ranging from -~~66~~65% to -4% for each month (September to June) over 1992-2016 (Table 7). The largest and smallest reduction were about 6~~5.8~~4.67% and 4.30~~2~~%, which occurred in June and March, respectively. Variation analysis of monthly average snow mass could offer a powerful evidence for annual average snow mass exhibit a significantly decreasing tendency (Table 7, Fig. 10B).

Over large areas, it is extremely convenient to use remote sensing to infer SWE. Albeit there are numerous ways to estimate SWE, it is very challenging to determine precise distributions of SWE at regional and global scales (Chang et al., 1987;Kongoli, 2004;Tedesco and Narvekar, 2010;Bair et al., 2018). Snow density, which can be used to convert SWE from SD, is potential and key factor in accurate estimation of SWE (Sturm et al., 2010;Tedesco and Narvekar, 2010). In fact, snow density typically varies from 0.05 g/cm^3 for new snow at low air temperatures to over 0.55 g/cm^3 for a ripened snowpack (Anderton et al., 2004;Cordisco et al., 2006). Noteworthily, this study using dynamic snow density to convert SD to SWE is based on the assumption that snowpack occurs as a single layer (Sturm et al., 2010), to capture dynamic characteristics of snow property. The evolution of the ephemeral snow class did not be provided by Sturm et al. (2010). The mean value (0.25 g/cm^3) of snow density of ephemeral snow (Zhong et al., 2014), which mean that without any evolution throughout the snow cover year. Meanwhile, this value for ephemeral snow was set as 0.2275 g/cm^3 in Tedesco and Jeyaratnam (2016) study. Snow density also exhibits great heterogeneity in vertical direction, so that a single layer of snow concept cannot fully capture the snowpack property. The density of the top snowpack (fresh snow; ~ 0.10 g/cm^3) increases gradually from the top toward the bottom (Dai et al., 2012). The bottom layer of snowpack is old undergoing compaction and grain size growth with a relatively high density (0.3~0.6 g/cm^3). Although our snow density description strategy does not completely describe the actual evolution in snow density, there is no better alternative.

4.3 Snow cover days

Snow cover days (SCD) is defined as the number of days in one snow cover year in which SD is over 0 cm (Zhong, 2014). Snow cover year was defined as the period between July of a given year and

June of the following year (Xiao et al., 2018). A least-squares regression was used to analyze the variation of SCD for each pixel from 24 snow cover years, with per-pixel evaluation of significance (F-test).

We exploring the variation in SCD during 1992-2016. Most areas across the Northern Hemisphere present a prominently decreasing trend at a rate ranging from 0 to 5 day $yr.^{-1}$ (Fig. 11a). Decreasing regions are mainly distributed in EU. For example, north of Russia and large parts of central Asia. The area that shows decreasing trends of SCD in EU is much larger than that in NA (Fig. 11a) (Derksen and Brown, 2012). Areas that the decrease at a rate greater than 5 day $yr.^{-1}$ are almost all located in China, such as North of Qilian Mountain, central Tibetan Plateau, and Tianshan Mountain. Areas that exhibits increasing trends, can be found in central of NA, Western Europe, Northwestern Mongolia, and some parts of China. Throughout the Northern Hemisphere (Fig. 11b), the decreasing trend covered most parts of the regions (25 ~ 85 °N) with a mean decreasing rate of approximately 1.0 day $yr.^{-1}$. Latitudes around 50 °N is an exception where variation is close to 0 day $yr.^{-1}$. The most notable variation trend (decreasing or increasing) occurred over polar region (Fig. 11b). This may be because there are few pixels in the polar mainland.

SCD variation rate also were divided into 5 grade (Table 5). Unlike SCD variation rate patterns, the variation level pattern shows that the non-significant changes area dominates SCD variation trends across the Northern Hemisphere (Fig. 11c). Extremely significant and significant decrease appear in northwest of Hudson Bay in Canada, Kamchatka peninsula, Eastern European plains, the north of Russia, Iranian plateau, and several regions in China (the Tibet Plateau, Tianshan Mountain and Northeast China Plain). In addition, extremely significant and significant increase only occur in a limited area of NA, eastern Tibet Plateau regions, and China's central and northern regions.

Interestingly, the opposite variation trends in SCD and SD appear in several regions. Maximum SD in spring (Fig. 8c) and annual average SD (figure not shown) show extremely significant increasing trends , whereas SCD exhibit extremely significant decreases in corresponding regions (Fig. 11c), such as Central Siberian Plateau, Greater Khingan Mountains in China, and the eastern Scandinavian Peninsula. This different variation trend of SD and SCD was also reported by Zhong et al. (2018) using ground-based data. The primary reason may be the increase of frequency of extreme snowfall in which SD could demonstrate on increasing trend. Additionally, a recent study found that the greater SWE, the faster melting rate leading to a shortened SCD in Northern Hemisphere (Wu et al., 2018).

Despite the similarities between the station- and satellite-derived time series, it can be demonstrated that Northern Hemisphere meteorological station data do not provide perfect large-scale variation characteristics of ground snow cover (Zhong et al., 2018). Our analyses provide further evidence supporting observations of significant decreasing trends in SCD occurring in the Northern Hemisphere. Compared to SCD derived from optic sensors snow cover product, however, the specific quantity of SCD and SCD variation rate derived from NHSnow SD data was overestimated (Wang et al., 2018;Hori et al., 2017). The SCD variation trends derived from NHSnow product almost is same as derived from optical snow cover product in variation pattern (Hori et al., 2017).

Since the optical (MODIS or AVHRR) and microwave sensors (SSM/I or AMSR-E) respond in different parts of the electromagnetic spectrum, the estimated snow cover will to be somewhat vary. The shallow snow could not induce volume scattering at 37 GHz, and thus passive microwave observations often give better snow cover result at thick snow (>5 cm) (Foster et al., 2009;Wang et al., 2008). The threshold for SCD definition in here is 0 cm, whereas it is 1 cm or larger in other studies (Ke et al., 2016;Dyer and Mote, 2006). As well, another explanation for these discrepancy could be snow cover identification algorithm (Liu et al., 2018;Hall et al., 2002).

The microwave radiation characteristics of snow cover is similar to that of precipitation, cold desert and, frozen ground (Grody and Basist, 1996). Commission and omission errors in NHSnow product may result from coarse spatial resolution, snow characteristics and topography according to Dai et al. (2017), precipitation (Liu et al., 2018;Grody and Basist, 1996) especially over frozen ground (Tsutsui and Koike, 2012). Algorithm several rules were used to distinguish snow from precipitation, cold desert, and frozen ground (Xiao et al., 2018), it is impossible to entirely remove interference factors in each image. Additionally, the precondition of NHSnow is dry snow, which mean almost no wet snow was considered into SCD variation analysis (Singh and Gan, 2000). The poorer performance of the microwave derived products was anticipated because of documented difficulties monitoring snow cover over forested and mountainous terrain (Vander Jagt et al., 2013;Smith and Bookhagen, 2016).

5 Conclusions

This project applied the SVR SD retrieval algorithm proposed by Xiao et al (2018), which using

PM remote sensing and other auxiliary data, to develop a long term (from January 1992 to December 2016) Northern Hemisphere daily SD and SWE products (NHSnow) with 25-km spatial resolution. We then analyzed the spatial and temporal change in snow cover (SD, ~~total SWE~~snow mass and, SCD) across the Northern Hemisphere, and quantified the magnitude of variation of snow cover using SD and SWE extracted from NHSnow product.

In this study, we validated and compared among daily gridded products (NHSnow, GlobSnow and ERA-Interim/Land) against ground snow-depth observations. The results show relatively high estimation accuracy of SD from NHSnow, providing the relatively little bias, RMSE, and MAE between the newly SD products and in situ observation. Analysis of SD variation revealed that the variation rate ranging from 0 to 1 cm yr.$^{-1}$ (negative and positive) dominates the change in the Northern Hemisphere, and the maximum changes appear in winter. Additionally, the results revealed the overall SD trends in three seasons show increasing trend during 1992–2001, however it has a decreasing trend during 2002–2016. Similar conclusions also appear in ~~total SWE~~snow mass change analysis. The ~~total SWE~~annual maximum, average and minimum snow mass exhibit significantly decrease trends and respectively show~~s~~ a 8%, 13~~2.5~~% and 67% reduction. ~~and t~~The monthly average snow mass has shown a decreasing trend almost in every month~~m onthly average total SWE~~ and the reduction range from~~is~~ 64.67~~65.8~~% (June) to~~for the largest reduction and a~~ 4.3~~2~~% (March)~~for least reduction which occur in June and March, respectively~~. The ~~total SWE~~annual average snow mass report well-documented significant decreasing trends (~20 km^3 yr.$^{-1}$, $P < 0.05$) during the study period. Regression analysis multi-year Northern Hemisphere SCD exhibits a prominent decreasing trend at a rate ranging from 0 to 5 day yr.$^{-1}$. The area of decreasing trends of SCD in EU is much larger than in NA. Unlike the SCD variation rate, its variation level shows that non-significant changes areas dominate the variation pattern across the Northern Hemisphere. An abnormal and interesting phenomenon is that opposite SCD and SD variation trends appear in several regions.

While this study shed light on the spatiotemporal variability trends of snow cover across the Northern Hemisphere using 25-year NHSnow product, we cannot claim NHSnow dataset could completely capture the climate change signal in each region and season. Because of the deficiencies and limitations (e.g. overestimation, underestimation), further efforts should be made to improve the estimation accuracy and robustness of the SD inversion algorithm. Additionally, when more reliable and numerous data become available, we will do more comprehensive validation over higher latitudes and mountainous regions (Dai et al., 2017). Meanwhile, the validation analysis also should be carried out in complex terrain and different land cover types (Tennant et al., 2017;Snauffer et al., 2016). It is recommended that future work focus on the climatic effects and climatological causes in snow cover changes to comprehensively understand the associated snow cover change mechanisms against a climate change background (Huang et al., 2017;Flanner et al., 2011;Cohen et al., 2012).

Acknowledgments

This study was funded by the National Natural Science Foundation of China (grant nos. 91325202; 41871050; 41801028), National Key Scientific Research Program of China (grant no. 2013CBA01802), and the Strategic Priority Research Program of Chinese Academy of Sciences (grant nos. XDA20100103; XDA20100313).

Appendix

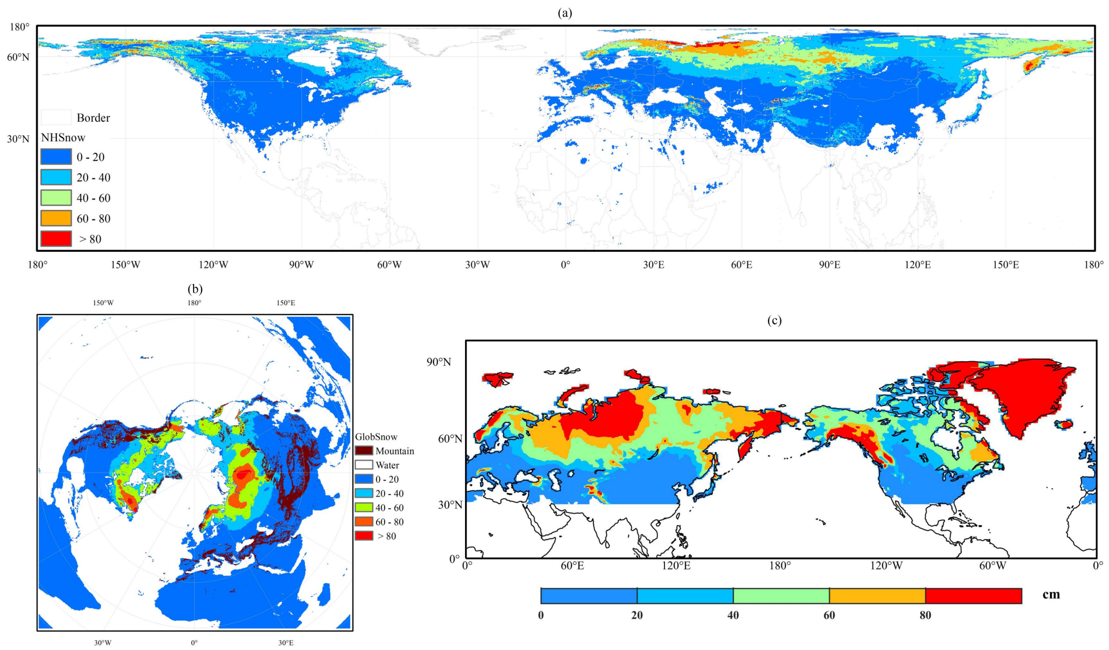

Figure A. Monthly average snow depth climatology of three products in February during 1992-2010: a) NHSnow; b) GlobSnow, c) ERA-Interim/Land

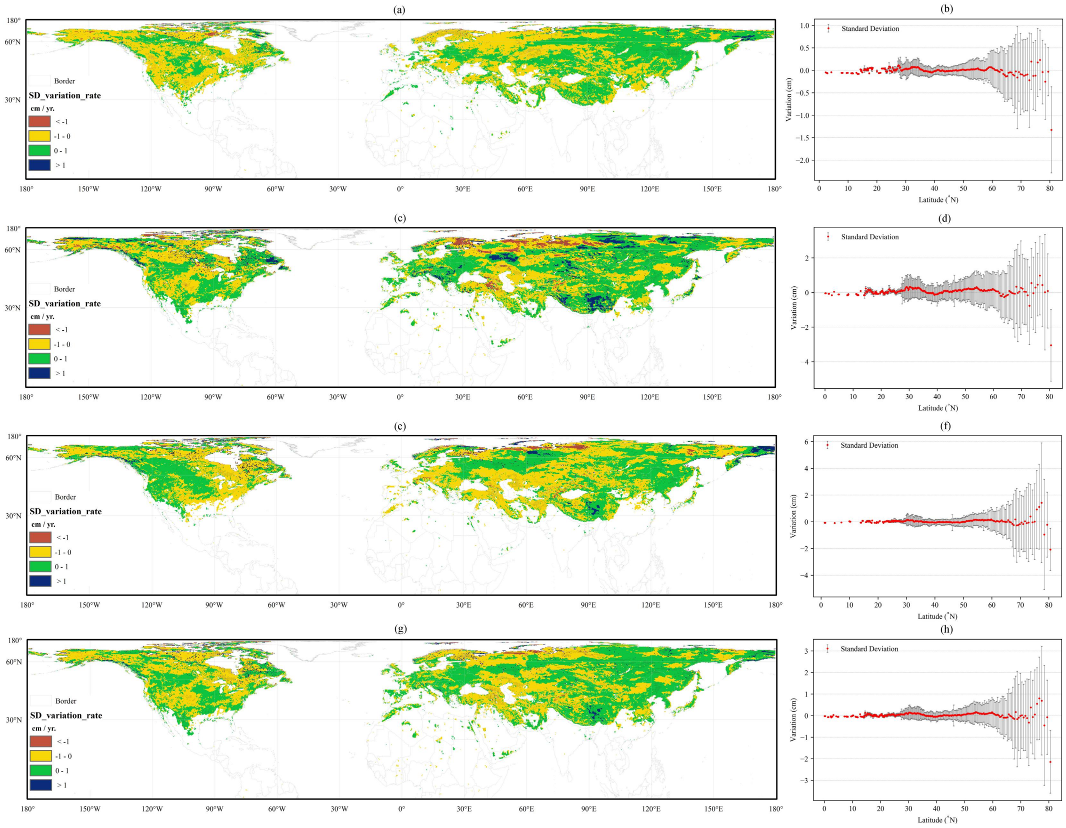

Figure B. The variation rate pattern of annual average (season) SD over the Northern Hemisphere for three snow cover season, fall (a, b; September to November), winter (c, d; December to February), spring (e, f; March to June) from 1992-2001. Black dots in (a, c, e, g) indicate that the changes are significant at 95% confidence level (CL). The zonal distribution in (b, d, f, h) are mapped at 0.25 degree resolution in latitude. The error bars in (b, d, f, h) is one times of standard deviation.

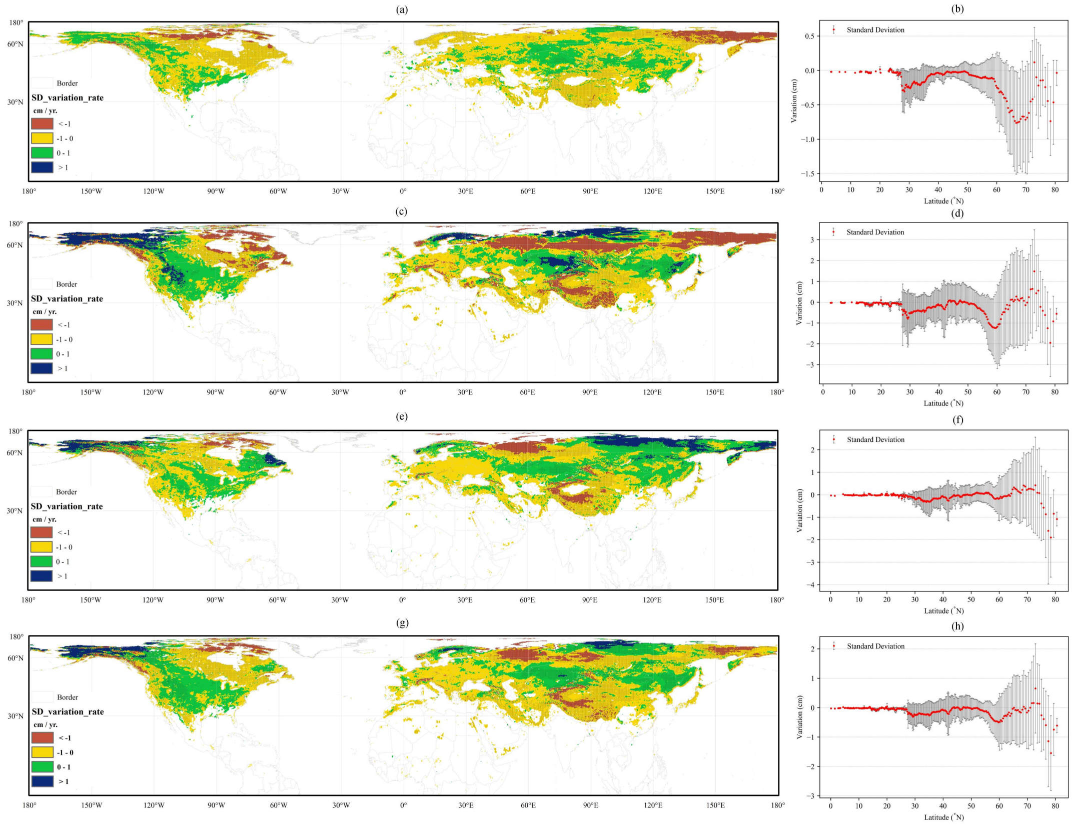

Figure C. The variation rate pattern of annual (season) average SD over the Northern Hemisphere for three snow cover season, fall (a, b; September to November), winter (c, d; December to February), spring (e, f; March to June) from 2002-2016. Black dots in (a, c, e, g) indicate that the changes are significant at 95% confidence level (CL). The zonal distribution in (b, d, f, h) are mapped at 0.25 degree resolution in latitude. The error bars in (b, d, f, h) is one times of standard deviation.

Table A. AVHRR Global Land Cover classification and reclassification schemes

Value	Classification Label	Reclassification Label
0	Water	Water
1	Evergreen needle leaf forest	Forest
2	Evergreen broad leaf forest	
3	Deciduous needle leaf forest	
4	Deciduous broad leaf forest	
5	Mixed forest	
6	Woodland	
7	Wooded grassland	Prairie (Grassland)
10	Grassland	
8	Closed shrub land	Shrub
9	Open shrub land	
11	Cropland	Bare-land
12	Bare ground	
13	Urban and built	

References

Amante, C., Eakins, B.W.: ETOPO1 1 arc-minute global relief model: procedures, data sources and analysis, US Department of Commerce, National Oceanic and Atmospheric Administration, National Environmental Satellite, Data, and Information Service, National Geophysical Data Center, Marine Geology and Geophysics Division Colorado, 2009.

Anderton, S. P., White, S. M., and Alvera, B.: Evaluation of spatial variability in snow water equivalent for a high mountain catchment, Hydrological Processes, 18, 435-453, 10.1002/hyp.1319, 2004.

Armstrong, R., and Brodzik, M.: An earth-gridded SSM/I data set for cryospheric studies and global change monitoring, Advances in Space Research, 16, 155-163, 1995.

Armstrong, R. L., Knowles, K.W., Brodzik, M.J., Hardman, M.A.: DMSP SSM/I pathfinder daily EASE-grid brightness temperatures, Boulder, Colorado USA: National snow and ice data center, Digital media, 2008.

Bair, E. H., Andre Calfa, A., Rittger, K., and Dozier, J.: Using machine learning for real-time estimates of snow water equivalent in the watersheds of Afghanistan, The Cryosphere, 12, 1579-1594, 10.5194/tc-12-1579-2018, 2018.

Balsamo, G., Albergel, C., Beljaars, A., Boussetta, S., Brun, E., Cloke, H., Dee, D., Dutra, E., Munoz-Sabater, J., and Papenberger, F.: ERA-Interim/Land: A global land surface reanalysis dataset, European Geosciences Union General Assembly, 2015, 389-407,

Barnett, T. P., Adam, J. C., and Lettenmaier, D. P.: Potential impacts of a warming climate on water availability in snow-dominated regions, Nature, 438, 303-309, 10.1038/nature04141, 2005.

Barrett, B. S., Henderson, G. R., and Werling, J. S.: The Influence of the MJO on the Intraseasonal Variability of Northern Hemisphere Spring Snow Depth, Journal of Climate, 28, 7250-7262, 10.1175/jcli-d-15-0092.1, 2015.

Bilello, M. A.: Regional and seasonal variations in snow-cover density in the U.S.S.R, 1984.

Brodzik, M. J., and Knowles, K.: EASE-Grid: A Versatile Set of Equal-Area Projections and Grids, 2002.

Brown, R., Derksen, C., and Wang, L.: A multi-data set analysis of variability and change in Arctic spring snow cover extent, 1967–2008, Journal of Geophysical Research, 115, 10.1029/2010jd013975, 2010.

Brown, R., and Robinson, D.: Northern Hemisphere spring snow cover variability and change over 1922–2010 including an assessment of uncertainty, The Cryosphere, 5, 219-229, 2011.

Brown, R. D., and Frei, A.: Comment on “Evaluation of surface albedo and snow cover in AR4 coupled models” by A. Roesch, Journal of Geophysical Research, 112, 10.1029/2006jd008339, 2007.

Chang, A., Foster, J., and Hall, D.: Nimbus-7 SMMR derived global snow cover parameters, Ann. Glaciol, 9, 39-44, 1987.

Che, T., Xin, L., Jin, R., Armstrong, R., and Zhang, T.: Snow depth derived from passive microwave remote-sensing data in China, Annals of Glaciology, 49, 145-154, 2008.

Che, T., Dai, L., Zheng, X., Li, X., and Zhao, K.: Estimation of snow depth from passive microwave brightness temperature data in forest regions of northeast China, Remote Sensing of Environment, 183, 334-349, 2016.

Cohen, J. L., Furtado, J. C., Barlow, M. A., Alexeev, V. A., and Cherry, J. E.: Arctic warming, increasing snow cover and widespread boreal winter cooling, Environmental Research Letters, 7, 10.1088/1748-9326/7/1/014007, 2012.

Cordisco, E., Prigent, C., and Aires, F.: Snow characterization at a global scale with passive microwave

satellite observations, Journal of Geophysical Research, 111, 10.1029/2005jd006773, 2006.
Dai, L., Che, T., Wang, J., and Zhang, P.: Snow depth and snow water equivalent estimation from AMSR-E data based on a priori snow characteristics in Xinjiang, China, Remote Sensing of Environment, 127, 14-29, 2012.
Dai, L., Che, T., and Ding, Y.: Inter-calibrating SMMR, SSM/I and SSMI/S data to improve the consistency of snow-depth products in China, Remote Sensing, 7, 7212-7230, 2015.
Dai, L., Che, T., Ding, Y., and Hao, X.: Evaluation of snow cover and snow depth on the Qinghai–Tibetan Plateau derived from passive microwave remote sensing, The Cryosphere, 11, 1933-1948, 10.5194/tc-11-1933-2017, 2017.
Derksen, C., Walker, A., and Goodison, B.: Evaluation of passive microwave snow water equivalent retrievals across the boreal forest/tundra transition of western Canada, Remote Sensing of Environment, 96, 315-327, 2005.
Derksen, C., and Brown, R.: Spring snow cover extent reductions in the 2008-2012 period exceeding climate model projections, Geophysical Research Letters, 39, n/a-n/a, 10.1029/2012gl053387, 2012.
Diffenbaugh, N. S., Scherer, M., and Ashfaq, M.: Response of snow-dependent hydrologic extremes to continued global warming, Nat Clim Chang, 3, 379-384, 10.1038/nclimate1732, 2013.
Dutra, E., Balsamo, G., Viterbo, P., Miranda, P. M. A., Beljaars, A., Schär, C., and Elder, K.: An improved snow scheme for the ECMWF land surface model: description and offline validation, Journal of Hydrometeorology, 11, 899-916, 2010.
Dyer, J. L., and Mote, T. L.: Spatial variability and trends in observed snow depth over North America, Geophysical Research Letters, 33, 10.1029/2006gl027258, 2006.
Flanner, M. G., Shell, K. M., Barlage, M., Perovich, D. K., and Tschudi, M. A.: Radiative forcing and albedo feedback from the Northern Hemisphere cryosphere between 1979 and 2008, Nature Geoscience, 4, 151-155, 10.1038/ngeo1062, 2011.
Forman, B. A., Reichle, R. H., and Derksen, C.: Estimating Passive Microwave Brightness Temperature Over Snow-Covered Land in North America Using a Land Surface Model and an Artificial Neural Network, IEEE Transactions on Geoscience & Remote Sensing, 52, 235-248, 2013.
Forman, B. A., and Reichle, R. H.: Using a support vector machine and a land surface model to estimate large-scale passive microwave brightness temperatures over snow-covered land in North America, IEEE Journal of Selected Topics in Applied Earth Observations and Remote Sensing, 8, 4431-4441, 2015.
Foster, J., Chang, A., and Hall, D.: Comparison of snow mass estimates from a prototype passive microwave snow algorithm, a revised algorithm and a snow depth climatology, Remote sensing of environment, 62, 132-142, 1997.
Foster, J. L., Hall, D. K., Kelly, R. E. J., and Chiu, L.: Seasonal snow extent and snow mass in South America using SMMR and SSM/I passive microwave data (1979–2006), Remote Sensing of Environment, 113, 291-305, 10.1016/j.rse.2008.09.010, 2009.
Foster, J. L., Hall, D. K., Eylander, J. B., Riggs, G. A., Nghiem, S. V., Tedesco, M., Kim, E., Montesano, P. M., Kelly, R. E. J., Casey, K. A., and Choudhury, B.: A blended global snow product using visible, passive microwave and scatterometer satellite data, International Journal of Remote Sensing, 32, 1371-1395, 10.1080/01431160903548013, 2011.
Frei, A., Tedesco, M., Lee, S., Foster, J., Hall, D. K., Kelly, R., and Robinson, D. A.: A review of global satellite-derived snow products, Advances in Space Research, 50, 1007-1029, 10.1016/j.asr.2011.12.021, 2012.

Friedl, M. A., Sulla-Menashe, D., Tan, B., Schneider, A., Ramankutty, N., Sibley, A., and Huang, X.: MODIS Collection 5 global land cover: Algorithm refinements and characterization of new datasets, Remote Sensing of Environment, 114, 168-182, 2010.
Friedl, M. A., and Sulla-Menashe, D.: Note to users of MODIS Land Cover (MCD12Q1) Products, Report. Accessed March, 2, 2014, 2011.
Gan, T. Y., Barry, R. G., Gizaw, M., Gobena, A., and Balaji, R.: Changes in North American snowpacks for 1979–2007 detected from the snow water equivalent data of SMMR and SSM/I passive microwave and related climatic factors, Journal of Geophysical Research: Atmospheres, 118, 7682-7697, 2013.
Gharaei-Manesh, S., Fathzadeh, A., and Taghizadeh-Mehrjardi, R.: Comparison of artificial neural network and decision tree models in estimating spatial distribution of snow depth in a semi-arid region of Iran, Cold Regions Science and Technology, 122, 26-35, 2016.
Goïta, K., Walker, A. E., and Goodison, B. E.: Algorithm development for the estimation of snow water equivalent in the boreal forest using passive microwave data, International Journal of Remote Sensing, 24, 1097-1102, 2003.
Grippa, M., Mognard, N., Le Toan, T., and Josberger, E.: Siberia snow depth climatology derived from SSM/I data using a combined dynamic and static algorithm, Remote sensing of environment, 93, 30-41, 2004.
Grody, N. C., and Basist, A. N.: Global identification of snowcover using SSM/I measurements, IEEE Transactions on geoscience and remote sensing, 34, 237-249, 1996.
Hall, D. K., Kelly, R. E. J., Riggs, G. A., Chang, A. T. C., and Foster, J. L.: Assessment of the relative accuracy of hemispheric-scale snow-cover maps, Annals of Glaciology, 34, 24-30, 2002.
Hancock, S., Baxter, R., Evans, J., and Huntley, B.: Evaluating global snow water equivalent products for testing land surface models, Remote sensing of environment, 128, 107-117, 10.1016/j.rse.2012.10.004, 2013.
Hansen, M. C., Defries, R. S., Townshend, J. R. G., and Sohlberg, R.: Global land cover classification at 1 km spatial resolution using a classification tree approach, International Journal of Remote Sensing, 21, 1331-1364, 2000.
Hori, M., Sugiura, K., Kobayashi, K., Aoki, T., Tanikawa, T., Kuchiki, K., Niwano, M., and Enomoto, H.: A 38-year (1978–2015) Northern Hemisphere daily snow cover extent product derived using consistent objective criteria from satellite-borne optical sensors, Remote Sensing of Environment, 191, 402-418, 10.1016/j.rse.2017.01.023, 2017.
Huang, X., Deng, J., Ma, X., Wang, Y., Feng, Q., Hao, X., and Liang, T.: Spatiotemporal dynamics of snow cover based on multi-source remote sensing data in China, The Cryosphere, 10, 2453-2463, 10.5194/tc-10-2453-2016, 2016.
Huang, X., Deng, J., Wang, W., Feng, Q., and Liang, T.: Impact of climate and elevation on snow cover using integrated remote sensing snow products in Tibetan Plateau, Remote Sensing of Environment, 190, 274-288, 10.1016/j.rse.2016.12.028, 2017.
Immerzeel, W. W., Van Beek, L. P., and Bierkens, M. F.: Climate Change Will Affect the Asian Water Towers, Science, 328, 1382-1385, 2010.
Ke, C.-Q., Li, X.-C., Xie, H., Ma, D.-H., Liu, X., and Kou, C.: Variability in snow cover phenology in China from 1952 to 2010, Hydrology and Earth System Sciences, 20, 755-770, 10.5194/hess-20-755-2016, 2016.
Kongoli, C.: Interpretation of AMSU microwave measurements for the retrievals of snow water equivalent and snow depth, Journal of Geophysical Research, 109, 10.1029/2004jd004836, 2004.

Li, W., Guo, W., Qiu, B., Xue, Y., Hsu, P. C., and Wei, J.: Influence of Tibetan Plateau snow cover on East Asian atmospheric circulation at medium-range time scales, Nat Commun, 9, 4243, 10.1038/s41467-018-06762-5, 2018.

Liang, J., Liu, X., Huang, K., Li, X., Shi, X., Chen, Y., and Li, J.: Improved snow depth retrieval by integrating microwave brightness temperature and visible/infrared reflectance, Remote Sensing of Environment, 156, 500-509, 2015.

Liu, X., Jiang, L., Wu, S., Hao, S., Wang, G., and Yang, J.: Assessment of Methods for Passive Microwave Snow Cover Mapping Using FY-3C/MWRI Data in China, Remote Sensing, 10, 10.3390/rs10040524, 2018.

Liu, Y., and Key, J. R.: Less winter cloud aids summer 2013 Arctic sea ice return from 2012 minimum, Environmental Research Letters, 9, 10.1088/1748-9326/9/4/044002, 2014.

López-Moreno, J. I., Fassnacht, S. R., Beguería, S., and Latron, J. B. P.: Variability of snow depth at the plot scale: implications for mean depth estimation and sampling strategies, The Cryosphere, 5, 617-629, 10.5194/tc-5-617-2011, 2011.

Mudryk, L. R., Derksen, C., Kushner, P. J., and Brown, R.: Characterization of Northern Hemisphere Snow Water Equivalent Datasets, 1981–2010, Journal of Climate, 28, 8037-8051, 10.1175/jcli-d-15-0229.1, 2015.

Pulliainen, J.: Mapping of snow water equivalent and snow depth in boreal and sub-arctic zones by assimilating space-borne microwave radiometer data and ground-based observations, Remote Sensing of Environment, 101, 257-269, 2006.

Qin, D., Liu, S., and Li, P.: Snow cover distribution, variability, and response to climate change in western China, J. Climate, 19, 1820-1833, 2006.

Robinson, D. A., and Frei, A.: Seasonal variability of Northern Hemisphere snow extent using visible satellite data, The Professional Geographer, 52, 307-315, 2000.

Rupp, D. E., Mote, P. W., Bindoff, N. L., Stott, P. A., and Robinson, D. A.: Detection and Attribution of Observed Changes in Northern Hemisphere Spring Snow Cover, Journal of Climate, 26, 6904-6914, 10.1175/jcli-d-12-00563.1, 2013.

Singh, P. R., and Gan, T. Y.: Retrieval of snow water equivalent using passive microwave brightness temperature data, Remote Sensing of Environment, 74, 275-286, 2000.

Smith, T., and Bookhagen, B.: Assessing uncertainty and sensor biases in passive microwave data across High Mountain Asia, Remote Sensing of Environment, 181, 174-185, 2016.

Snauffer, A. M., Hsieh, W. W., and Cannon, A. J.: Comparison of gridded snow water equivalent products with in situ measurements in British Columbia, Canada, Journal of Hydrology, 541, 714-726, 10.1016/j.jhydrol.2016.07.027, 2016.

Sturm, M., Holmgren, J., and Liston, G. E.: A seasonal snow cover classification system for local to global applications, Journal of Climate, 8, 1261-1283, 1995.

Sturm, M., Taras, B., Liston, G. E., Derksen, C., Jonas, T., and Lea, J.: Estimating snow water equivalent using snow depth data and climate classes, Journal of Hydrometeorology, 11, 1380-1394, 2010.

Sturm, M.: White water: Fifty years of snow research in WRR and the outlook for the future, Water Resources Research, 51, 4948-4965, 10.1002/2015wr017242, 2015.

Takala, M., Luojus, K., Pulliainen, J., Derksen, C., Lemmetyinen, J., Kärnä, J.-P., Koskinen, J., and Bojkov, B.: Estimating northern hemisphere snow water equivalent for climate research through assimilation of space-borne radiometer data and ground-based measurements, Remote Sensing of

Environment, 115, 3517-3529, 2011.

Tedesco, M., Pulliainen, J., Takala, M., Hallikainen, M., and Pampaloni, P.: Artificial neural network-based techniques for the retrieval of SWE and snow depth from SSM/I data, Remote sensing of Environment, 90, 76-85, 2004.

Tedesco, M., and Narvekar, P. S.: Assessment of the NASA AMSR-E SWE Product, IEEE Journal of Selected Topics in Applied Earth Observations and Remote Sensing, 3, 141-159, 2010.

Tedesco, M., Derksen, C., Deems, J. S., and Foster, J. L.: Remote sensing of snow depth and snow water equivalent, Remote Sensing of the Cryosphere, 73-98, 2014.

Tedesco, M., and Jeyaratnam, J.: A New Operational Snow Retrieval Algorithm Applied to Historical AMSR-E Brightness Temperatures, Remote Sensing, 8, 2016.

Tennant, C. J., Harpold, A. A., Lohse, K. A., Godsey, S. E., Crosby, B. T., Larsen, L. G., Brooks, P. D., Kirk, R. W. V., and Glenn, N. F.: Regional sensitivities of seasonal snowpack to elevation, aspect, and vegetation cover in western North America, Water Resources Research, 53, 2017.

Tilling, R. L., Ridout, A., Shepherd, A., and Wingham, D. J.: Increased Arctic sea ice volume after anomalously low melting in 2013, Nature Geoscience, 8, 643-646, 10.1038/ngeo2489, 2015.

Tsutsui, H., and Koike, T.: Development of Snow Retrieval Algorithm Using AMSR-E for the BJ Ground-Based Station on Seasonally Frozen Ground at Low Altitude on the Tibetan Plateau, Journal of the Meteorological Society of Japan. Ser. II, 90C, 99-112, 10.2151/jmsj.2012-C07, 2012.

Vander Jagt, B. J., Durand, M. T., Margulis, S. A., Kim, E. J., and Molotch, N. P.: The effect of spatial variability on the sensitivity of passive microwave measurements to snow water equivalent, Remote Sensing of Environment, 136, 163-179, 2013.

Wang, C., and Li, D.: Spatial-temporal variations of snow cover days and the maximum depth of snow cover in China during recent 50 years, Journal of Glaciology and Geocryology, 34, 247-256, 2012.

Wang, X., Xie, H., and Liang, T.: Evaluation of MODIS snow cover and cloud mask and its application in Northern Xinjiang, China, Remote Sensing of Environment, 112, 1497-1513, 10.1016/j.rse.2007.05.016, 2008.

Wang, Y., Huang, X., Liang, H., Sun, Y., Feng, Q., and Liang, T.: Tracking Snow Variations in the Northern Hemisphere Using Multi-Source Remote Sensing Data (2000–2015), Remote Sensing, 10, 10.3390/rs10010136, 2018.

Wegmann, M., Orsolini, Y., Dutra, E., Bulygina, O., Sterin, A., and Brönnimann, S.: Eurasian snow depth in long-term climate reanalyses, The Cryosphere, 11, 923-935, 10.5194/tc-11-923-2017, 2017.

Wentz, F. J.: SSM/I version-7 calibration report, Remote Sensing Systems Tech. Rep, 11012, 46, 2013.

Wu, X., Che, T., Li, X., Wang, N., and Yang, X.: Slower Snowmelt in Spring Along With Climate Warming Across the Northern Hemisphere, Geophysical Research Letters, 45, 12,331-312,339, 10.1029/2018gl079511, 2018.

Xiao, X., Zhang, T., Zhong, X., Shao, W., and Li, X.: Support vector regression snow-depth retrieval algorithm using passive microwave remote sensing data, Remote Sensing of Environment, 210, 48–64, 2018.

Xu, X., Liu, X., Li, X., Xin, Q., Chen, Y., Shi, Q., and Ai, B.: Global snow cover estimation with Microwave Brightness Temperature measurements and one-class in situ observations, Remote Sensing of Environment, 182, 227-251, 2016.

Xue, Y., and Forman, B. A.: Comparison of passive microwave brightness temperature prediction sensitivities over snow-covered land in North America using machine learning algorithms and the Advanced Microwave Scanning Radiometer, Remote Sensing of Environment, 170, 153-165, 2015.

Ye, H., Cho, H.-r., and Gustafson, P. E.: changes in russian winter snow accumulation during 1936-83 and its spatial patterns, Journal of Climate, 11, 856-863, 1998.
Yu, H., Zhang, X., Liang, T., Xie, H., Wang, X., Feng, Q., and Chen, Q.: A new approach of dynamic monitoring of 5 - day snow cover extent and snow depth based on MODIS and AMSR - E data from Northern Xinjiang region, Hydrological Processes, 26, 3052-3061, 2012.
Zhang, T., Osterkamp, T., and Stamnes, K.: Influence of the depth hoar layer of the seasonal snow cover on the ground thermal regime, Water Resources Research, 32, 2075-2086, 1996.
Zhang, T.: Influence of the seasonal snow cover on the ground thermal regime: An overview, Reviews of Geophysics, 43, 589-590, 2005.
Zhang, Y., Li, T., and Wang, B.: Decadal Change of the Spring Snow Depth over the Tibetan Plateau_ The Associated Circulation and Influence on the East Asian Summer Monsoon, Journal of Climate, 17, 2780-2793, 2004.
Zhong, X.: Spatiotemporal variability of snow cover and the relationship between snow and climate change across the Eurasian Contient, Lanzhou: Cold and Arid Regions Environmental and Engineering Research Institute, CAS, 2014.
Zhong, X., Zhang, T., and Wang, K.: Snow density climatology across the former USSR, The Cryosphere, 8, 785-799, 2014.
Zhong, X., Zhang, T., Kang, S., Wang, K., Zheng, L., Hu, Y., and Wang, H.: Spatiotemporal variability of snow depth across the Eurasian continent from 1966 to 2012, The Cryosphere, 12, 227-245, 10.5194/tc-12-227-2018, 2018.

List of Tables and Figures

Table 1 Detail description for SSM/ and SSMIS sensors. H and V denotes horizontal and vertical polarization, respectively.

Satellite	SSM/I		SSMIS
Platform	F 11	F 13	F 17
Temporal coverage	1991.12-1995.5	1995.5-2008.6	2006.12 -
Channels (GHz)	19 H, V; 22 V; 37 H, V; 85 H, V		19 H, V; 22 V; 37 H, V; 91 H, V

Table 2. Training sample filter rules

Layer ID	Filter rules
Layer2.	If $\text{Number}_{total}(layer2) \leq 3000$ $\text{Number}_{training}(layer2) = (\text{Number}_{total}(layer2))/2$ Else $\text{Number}_{training}(layer2) = 3000$
Layer3.	If $\text{Number}_{total}(layer3) \leq 3000$ $\text{Number}_{training}(layer3) = (\text{Number}_{total}(layer3))/2$ Else $\text{Number}_{training}(layer3) = 3000$
Layer1.	If $\text{Number}_{training}(layer2) > 2000$ or $\text{Number}_{training}(layer3) > 1000$ $\text{Number}_{training}(layer1)$ $= 15000 - \text{Number}_{training}(layer2) - \text{Number}_{training}(layer3)$ Else $\text{Number}_{training}(layer1) = 12000$

Table 3 Snow density estimation model parameters

Snow class	ρ_{max}	ρ_0	k_1	k_2	References
Alpine	0.5975	0.2237	0.0012	0.0038	Sturm et al. (2010)
Maritime	0.5979	0.2578	0.0010	0.0038	
Prairie	0.5940	0.2332	0.0016	0.0031	
Tundra	0.3630	0.2425	0.0029	0.0049	
Taiga	0.2170	0.2170	0	0	
Ephemeral	0.2500	0.2500	0	0	Zhong et al. (2014)

Table 4. The evaluated indexes (bias, MAE, RMSE; unit: cm) for three gridded SD products (NHSnow, GlobSnow, ERA-Interim/Land).

Products	Bias	MAE	RMSE
NHSnow	0.59	15.12	20.11
GlobSnow	1.19	15.98	15.48
ERA-Interim/Land	-5.60	18.72	37.77

Table 5. Rules of variation level grading

Variation rate	P value	Variation level
rate > 0	$p \leq 0.01$	extremely significant increase
rate > 0	$0.01 < p \leq 0.05$	significant increase
-	$P > 0.05$	non-significant change
rate < 0	$p \leq 0.01$	extremely significant decrease
rate < 0	$0.01 < p \leq 0.05$	significant decrease

Table 6. Mean variation rate of average SD (cm yr.$^{-1}$) over the Northern Hemisphere for three common period (1992-2016, 1992-2001, 2002-1996) and snow cover seasons (fall, winter, spring). Std. means standard deviation

Season	1992-2016 (Mean ± 1 Std.)	1992-2001 (Mean ± 1 Std.)	2002-2016 (Mean ± 1 Std.)
Fall	-0.08 ± 0.11	-0.01 ± 0.19	-0.15 ± 0.22
Winter	-0.11 ± 0.40	0.06 ± 0.62	-0.22 ± 0.75
Spring	-0.04 ± 0.25	0.02 ± 0.51	-0.07 ± 0.41
Year	-0.06 ± 0.20	0.02 ± 0.35	-0.11 ± 0.34

Table 7. Variation rate and changes of monthly average snow mass during 1992-2016. The asterisk indicate that the changes are significant at 95% confidence level

Month	Variation rate (km^3/yr.)	% Change in the mean of monthly average snow mass ~~over 1992-2016 period~~
September	-5.96*	-63.89%

October	-25.50*	-43.99%
November	-36.50*	-26.96%
December	-32.66*	-5.00%
January	-34.38*	-9.53%
February	-30.89*	-11.91%
March	1.90	-4.30%
April	-4.29	-6.46%
May	-11.33*	-19.59%
June	-8.01*	-64.67%

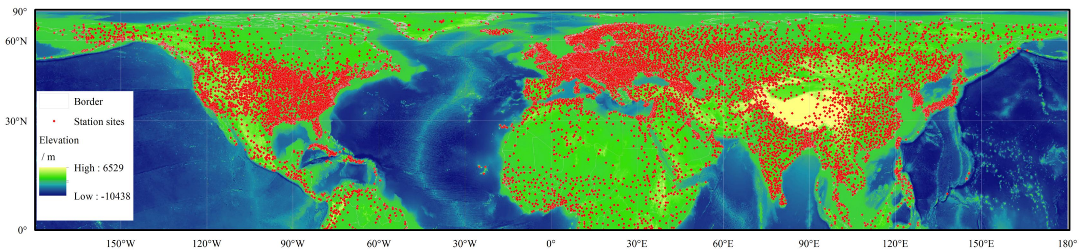

Figure 1. Distribution of Meteorological stations overlaid on ETOPO1 in the Northern Hemisphere.

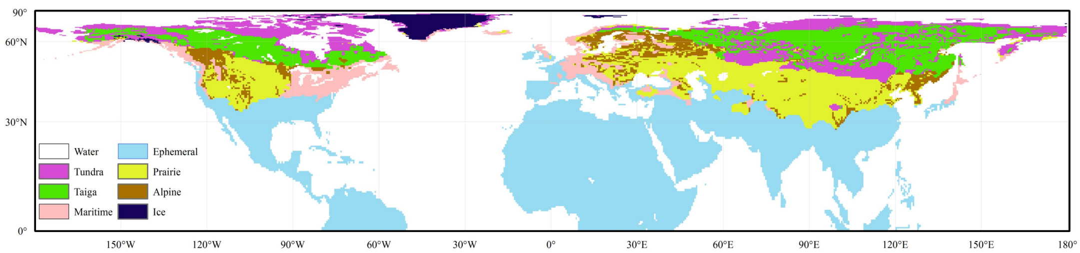

Figure 2. Snow Class distribution in the Northern Hemisphere

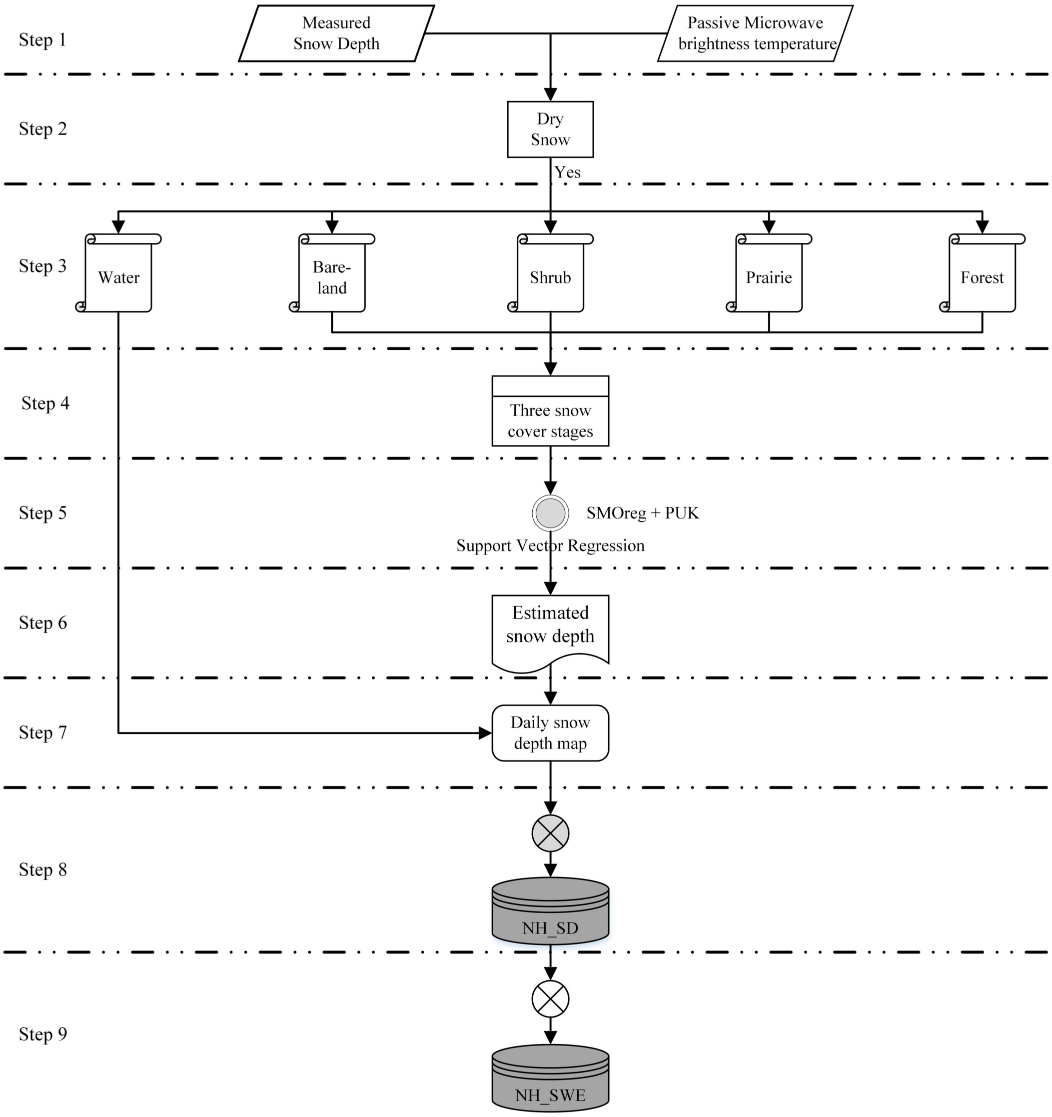

Figure 3. Process flowchart diagram for developing Northern Hemisphere daily snow depth and snow water equivalent data

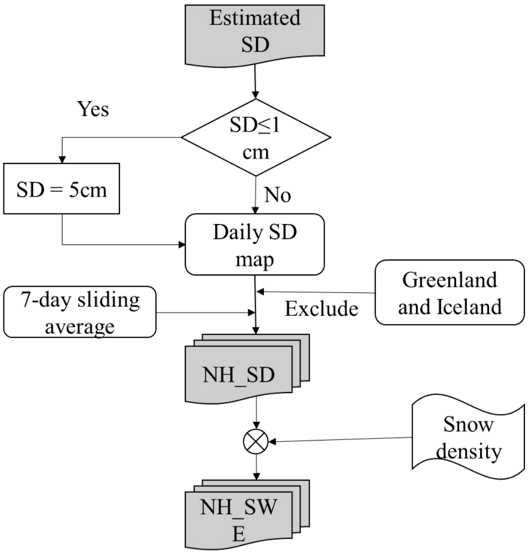

Figure 4. Flowchart diagram of the generation of NHSnow products.

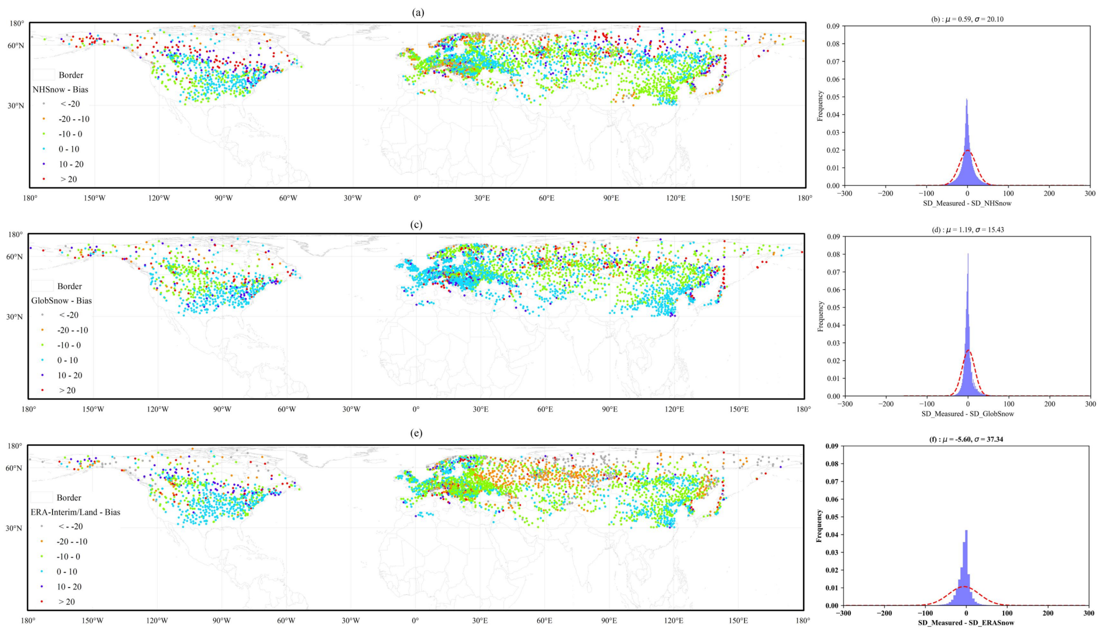

Figure 5. Bias of each meteorological station and histogram of biases for three products: a), b) NHSnow; c), d) GlobSnow, e), f) ERA-Interim/Land. The red dashed line in right column figures are the fitted normal distribution curve

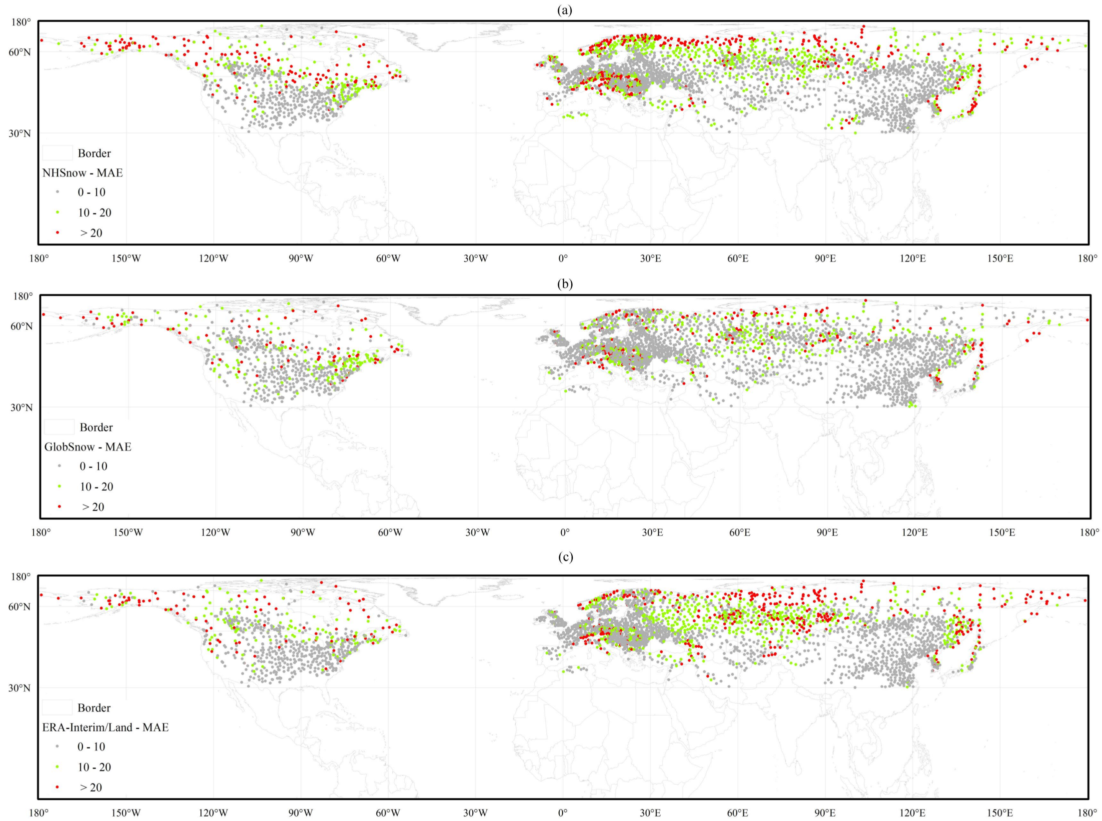

Figure 6. MAE of each meteorological station for three products: a) NHSnow, b) GlobSnow, c) ERA-Interim/Land.

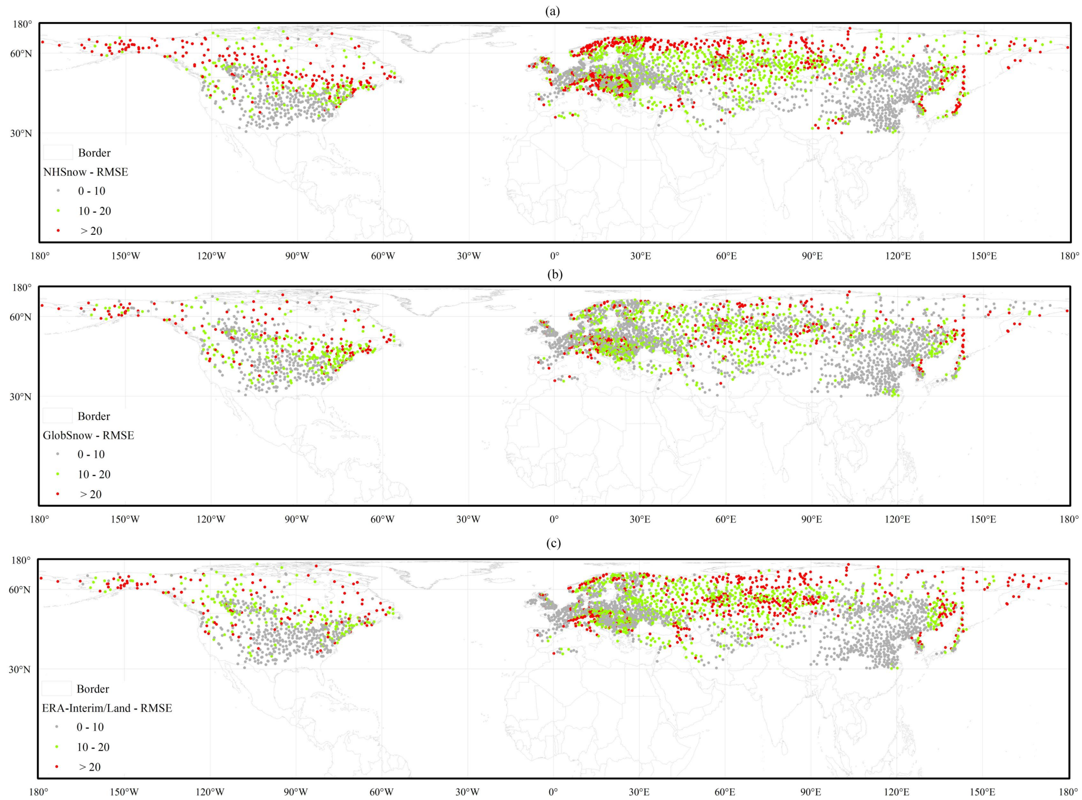

Figure 7. RMSE of each meteorological station for three products: a) NHSnow, b) GlobSnow, c)

ERA-Interim/Land.

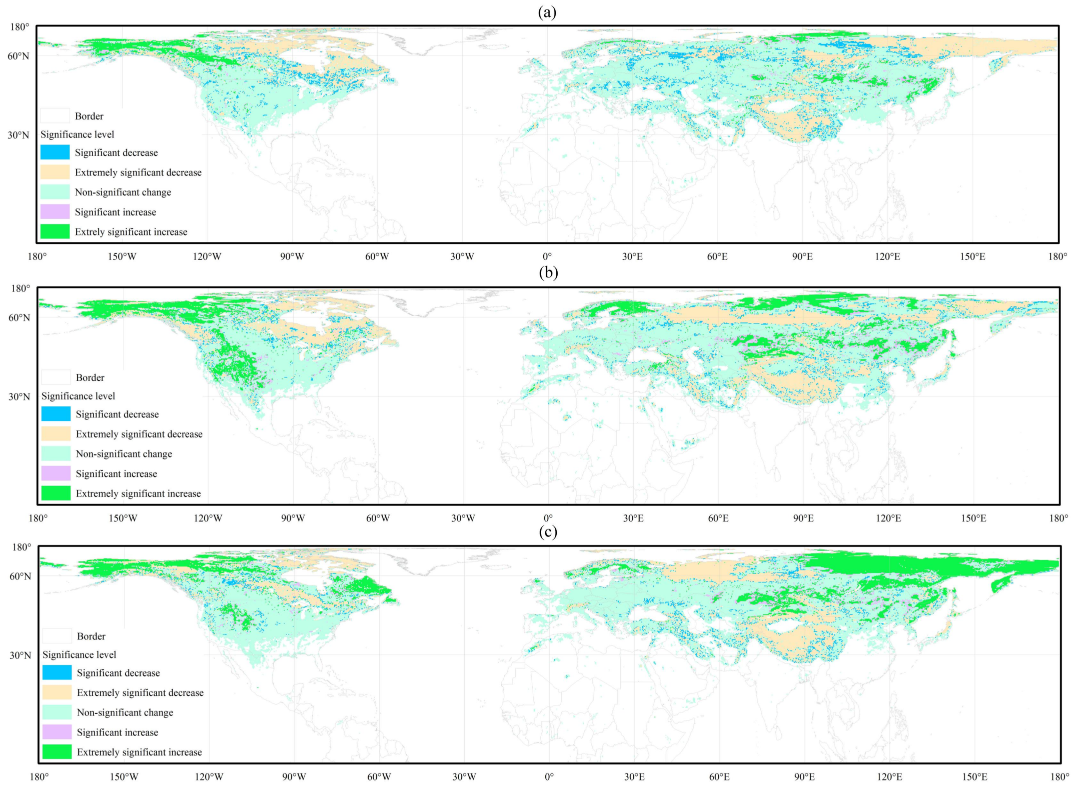

Figure 8. The variation rate pattern of season maximum SD with statistical significances over the Northern Hemisphere for three snow cover season, fall (a; September to November), winter (b; December to February), spring (c; March to June) from 1992-2016.

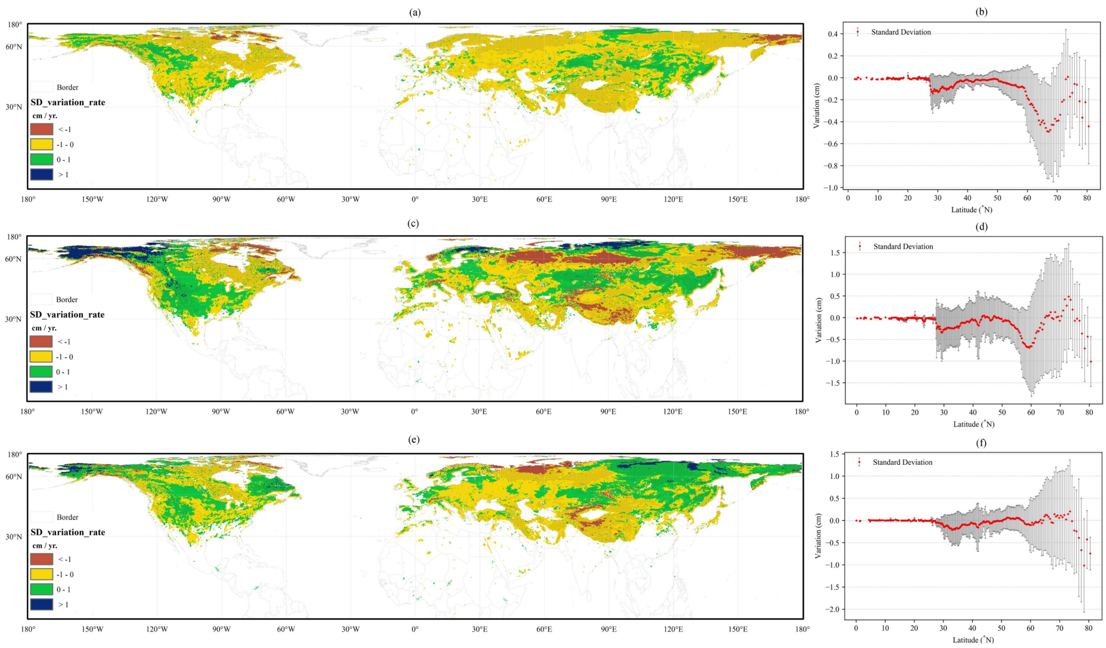

Figure 9. The variation rate pattern of season average SD over the Northern Hemisphere for three snow

cover season, fall (a, b; September to November), winter (c, d; December to February), spring (e, f; March to June) from 1992-2016. Black dots in (a, c, e) indicate that the changes are significant at 95% confidence level (CL). The zonal distribution in (b, d, f) are mapped at 0.25 degree resolution in latitude. The error bars in (b, d, f) is one times of standard deviation.

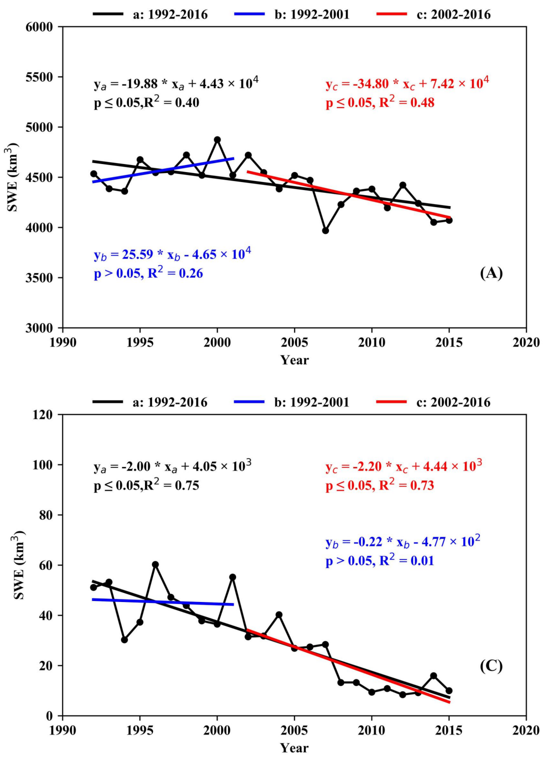

Figure 10. Interannual variation of annual maximum snow mass (A), annual average snow mass (B) and annual minimum snow mass (C) over the Northern Hemisphere for three period 1992-2016 (black line), 1992-2001 (blue line), and 2002-2016 (red line). Trends estimates were computed from least squares. P is the confidence level for the coefficient estimates; R^2 is the goodness of fit coefficient.

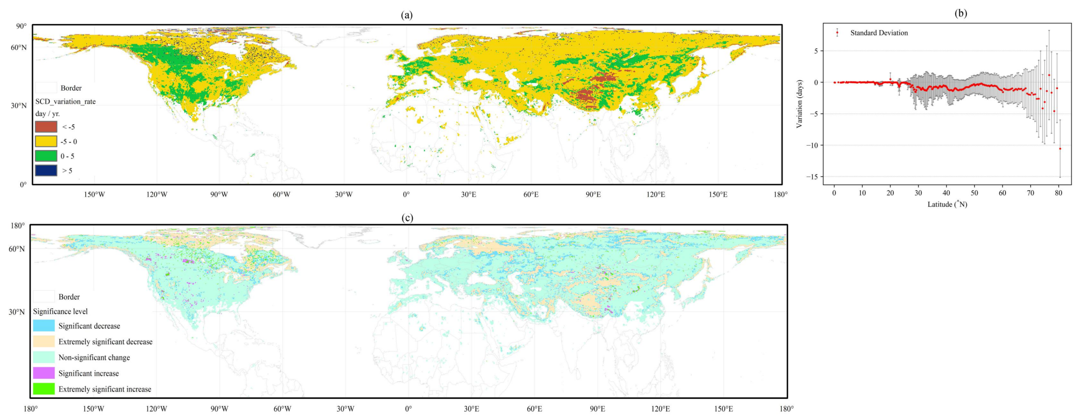

Figure 11. The variation rate pattern of SCD (a) and their statistical significances (c) over the Northern

Hemisphere from 1992-2016. The zonal distribution in (b) are mapped at 0.25 degree resolution in latitude. The error bars in (b) is one times of standard deviation.